CAPACITANCE MEASUREMENTS OF BULK SALINITY AND BRINE MOVEMENT IN FIRST-YEAR SEA ICE

By

Lars G. E. Backstrom

RECOMMENDED:

Advisory Committee Chair

Chair, Department of Geology and Geophysics

APPROVED:

Dean, College of Natural Science & Mathematics

Dean of the Graduate School

April 16, 2007

Date

CAPACITANCE MEASUREMENTS OF BULK SALINITY AND BRINE MOVEMENT IN FIRST-YEAR SEA ICE

Presented to the Faculty of the University of Alaska Fairbanks

In Partial Fulfillment of the Requirements for the Degree of

MASTER OF SCIENCE

By

Lars G. E. Backstrom, M.S.

Fairbanks, Alaska

May 2007

Abstract

Sea ice is an important component of the global climate system, as it changes the properties of the ocean-atmosphere interface. Understanding sea ice requires detailed knowledge of its temperature and bulk salinity. To measure these attributes using non-destructive in-situ techniques, instruments were frozen into first-year sea ice, and analysed jointly with ice-core, mass balance and climate data.

The bulk salinity of the ice is calculated from measurements of temperature and complex dielectric permittivity at 50 MHz in landfast ice in McMurdo Sound, Antarctica, the Chukchi Sea, Alaska, and in an outdoor tank experiment in Fairbanks, Alaska. A simple relation for estimating brine volume fraction and bulk salinity in columnar, bubble-free ice from the real part of the complex dielectric permittivity was derived. For relative brine volumes below 50-70 ‰ the error in the derived bulk salinity was below 15%.

The observed brine movement events are analyzed. The data clearly indicate the extent and impact of brine movement on ice temperature and salinity. The analysis of a drainage event recorded by both the temperature and dielectric permittivity probe provided insight into gravity drainage of brine driven by a large brine reservoir in the freeboard layer.

Table of Contents

Page

List of Figures

List of Tables

Acknowledgements

The research in this thesis has been supported by grant NSF-OPP 0126007 from the National Science Foundation. I would like to thank my supervisor, and co-author of the first chapter of my thesis, Dr. Hajo Eicken. I would also like to thank the members of my graduate committee, Drs. Nicole Molders, Vladimir Romanovsky, and Kenji Yoshikawa.

My thanks also go to Martin Iturri of Stevens Water Monitoring Systems and to Dr. Jeffrey Campbell for technical assistance with the Hydraprobe.

I want to thank the 2001-2002 staff at the New Zealand Scott Base, Antarctica, and the staff at the Barrow Arctic Science Consortium, Alaska, for their help with field-work and instrument maintenance.

I also thank Michael Tapp, and Patrick Cotter for help with laboratory work, and Dr. Daniel Pringle for help with the manuscript.

Finally, I thank my wife, Isabel, for her unfailing support.

General Introduction

Sea ice covers up to 7 % of the Earth's surface. A significant portion of it is first-year ice, or ice that is less than one year old, as opposed to multi-year ice that has survived one or more summers. Sea ice is a complex, semi-solid matrix formed by a combination of physical and chemical processes. The growth of sea ice is influenced by atmospheric, oceanic, and continental inputs (Dieckmann and Hellmer, 2003).

Sea ice might only be a thin layer, but it profoundly changes the surface properties of the ocean. It changes the ocean's albedo (Grenfell and Maykut, 1977; Grenfell and Perovich, 1984; Perovich, 1990; Perovich, 1994), as well as the dynamics of the ocean-atmosphere interface (Kottmeier and Sellmann, 1996). Together with its snow cover, it reduces the heating of the atmosphere by the ocean (Maykut, 1982; Ebert and Curry, 1993).

As the ice grows, it expels salt which helps drive the global oceanic thermohaline circulation (Aagard et al., 1981; Carmack, 2000). In addition, it poses a navigational hazard (Fogg, 2003), and is one of the largest biomes on Earth (Comiso, 2003).

Sea ice can be described by its temperature and bulk salinity, which control the brine volume fraction of the ice, as well as the morphology of the brine inclusions (Weeks and Ackley, 1986; Eicken, 2003). A knowledge of the total porosity of sea ice is important for the interpretation of its physical properties, e.g. thermal (Schwerdtfeger, 1963; Ono, 1975), mechanical (Weeks and Assur, 1967), and electromagnetical (Morey et al., 1984;

Grenfell et al., 1992; Hallikainen and Winebrenner, 1992; Eppler et al., 1992; Onstott, 1992).

Bulk salinity has been quite difficult to measure in naturally growing sea ice in the field. The most common method has been to measure the bulk salinity of melted core segments. However, since the study area can be remote and inaccessible, both the spatial and temporal resolution applying this approach tend to be limited.

The vertical salinity profile of multi-year sea ice has been analysed and modeled by Schwarzacher (1959) and Untersteiner (1968). Cox and Weeks (1988) developed a time-dependent simulation of the vertical salinity profile of first-year ice. However, the authors themselves point out that their model does not capture the significant horizontal variations in bulk salinity observed by Bennington (1967) and Tucker at al. (1984); neither does it simulate the changes in the vertical salinity profile due to rapid changes in meteorological conditions (Cox and Weeks, 1988).

As the ice initially forms, trapped seawater is encapsulated within the crystal matrix in the form of discrete brine inclusions. The brine inclusions form either between separate ice crystals, or as layers between ice lamellae parallel the ice crystal lattice. Close to the upper surface of the ice, brine inclusions tend to have random distribution, size, and shape, whereas in the interior of the ice they tend to form ellipsoids with their major axes aligned vertically. These inclusions change size with the changing temperature of the ice. The permeability of the ice increases non-linearly when the relative brine volume exceeds a so-called percolation thershold of 50-70‰ (Weeks and Ackley, 1986; Golden et al,

1998; Golden, 2001). The amount of entrained salt, and hence ice porosity, after initial formation is dependent on the thermal history of the ice cover (Cox and Weeks, 1988).

The vertical salinity profile of first-year sea ice is characteristically C-shaped (Malmgren, 1927) with higher bulk salinity at the upper and lower surfaces. This implies the existance of a large brine reservoir in the freeboard layer, which can create a hydraulic head as the ice warms in spring. This hydraulic head can drive gravity drainage (Eide and Martin, 1975), when interconnected networks of brine inclusions open up to the liquid ocean beneath the ice, and the cold dense brine, which is in thermal and haline equilibrium with its surrounding ice, percolates downwards (Eide and Martin, 1975).
In Chapter 1 of this thesis a method for estimating the relative brine volume and bulk salinity of sea ice from measurements of temperature and complex dielectric permittivity is presented. As part of the study, arrays of instruments were deployed in McMurdo Sound, Antarctica, and in the Chukchi Sea outside Barrow, Alaska. For comparison, probes measuring complex dielectric permittivity were also deployed in an outdoor tank experiment in Fairbanks, Alaska.

Vant (1976) completed an exhaustive study of the temperature and bulk salinity dependent complex dielectric properties of sea ice. By building on Vant's research it was possible to develop a model for estimating the relative brine volume and bulk salinity of bubble-free, columnar ice below the percolation threshold. The model is a good approximation of the interior of growing first-year sea ice. The method developed has centimeter resolution in space. The temporal resolution is set by the user.

For this study only the real part of the complex dielectric permittivity was examined in detail. By including the imaginary part of the complex dielectric permittivity the method can also be extended to determine the brine inclusion morphology of the ice (Morey et al., 1984).

In Chapter 2 of this thesis, the results and methods described in Chapter 1 are used to estimate the effect gravity drainage has on the heat budget of the ice. Data gathered between 1999 and 2003 from instruments frozen into the landfast sea ice in the Chukchi Sea outside of Barrow, Alaska, complemented with mass balance data, core samples, and measurements of complex dielectric permittivity are used to study the impact of gravity drainage events on the heat budget of the ice.

As the cold dense brine percolates down into warmer ice, it is no longer in haline equilibrium with the surrounding ice, which will melt, diluting the brine (Eide and Martin, 1975; Niedrauer and Martin, 1979; Worster and Wettlaufer, 1997).

The bulk salinity data from the cores as well as the temperature data make it possible to estimate the vertical relative brine volume profile of the ice, and how this volume varies with time. The instruments measure the temperature changes as the brine percolates downwards in the ice, and the brine melts the walls of the brine channel networks. The change in relative brine volume from the melting of the ice is recorded by the instruments measuring the complex dielectric permittivity. This experimental design allows for the estimation of the frequency and thermal impact of these events.

Chapter 1 Capacitance probe measurements of brine volume and bulk salinity in first-year sea ice[1]

1.1 Abstract

First-year sea ice plays an important role in the global climate system. It changes the physical properties of the surface of the polar oceans, and modifies the energy and mass transfer between the ocean and the atmosphere. An understanding of the way sea ice affects ocean–atmosphere exchange requires detailed knowledge of the evolution of ice physical properties, which are governed by its temperature and bulk salinity. To this effect, we assessed the utility of commercially available capacitance probes in determining the salinity evolution of first-year sea ice. Measurements of the complex dielectric permittivity, $\varepsilon=\varepsilon'-i\varepsilon''$, at 50 MHz were carried out in land-fast ice in McMurdo Sound, Antarctica, and inthe Chukchi Sea near Barrow, Alaska. For comparison, we also deployed the probes in artificial, young sea ice in an outdoor tank experiment in Fairbanks, AK. The dielectric permittivity data compare well with predictions from a dielectric mixture model.

---

[1] 1 Lars G.E. Backstrom, Hajo Eicken, Capacitance probe measurements of brine volume and bulk salinity in first-year sea ice, Cold Regions Science and Technology (2006), doi:10.1016/j.coldregions.2006.08.018.

We have derived a simple relation that allows for the derivation of brine volume fraction and bulk salinity in columnar first-year sea ice from the real part of the complex dielectric permittivity. For ice at temperatures below the percolation threshold, the error in the derived bulk salinity is less than 15%. The dependence of dielectric permittivity on brine inclusion morphology needs to be taken into consideration, and measurements indicate that changes in pore morphology are recorded in the capacitance measurements. In this paper we use the real part, ε', of the complex dielectric permittivity to study the bulk salinity of bubble-free columnar ice. Further investigations, using the imaginary part of the complex dielectric permittivity, ε", will make it possible to use the same probes to measure the bulk salinity and pore morphology of other types of ice, e.g., frazil, platelet, and multi-year ice.

1.2 Introduction

At its maximum extent during Antarctic winter, sea ice covers approximately 7% of the Earth's surface, with first-year sea ice making up over 80% of the ice in the southern polar ocean, and about 45% of the ice in the Arctic Ocean (Comiso, 2003). It is only a thin layer, measured in meters, compared to the thousands of meters of unfrozen ocean beneath, but it profoundly changes the physical characteristics of the ocean surface. Sea ice increases the albedo of the ocean, decreases the amount of moisture, the amount of heat, and the momentum transferred between the ocean and the atmosphere. Sea ice,

therefore, plays an important part in the global climate system (Maykut, 1986; Bitz and Lipscomb, 1999). Since the ice cover is typically relatively thin, it is also very sensitive to perturbations in the atmosphere–ocean heat flux (Dieckmann and Hellmer, 2003).

The physical properties – thermal, mechanical, and electromagnetic – of sea ice are governed by its temperature and salinity, which control the volume fraction of brine within the ice matrix, as well as the morphology of brine inclusions (Weeks and Ackley, 1986; Eicken, 2003). Due to the inaccessibility of the ice cover, it is comparatively difficult to measure these properties in situ within naturally growing sea ice. The salinity in particular has hitherto been difficult to measure in the field. The easiest and most widespread method is to measure the bulk salinity from core samples. One drawback of this method, however, is brine drainage from porous ice (Cox and Weeks, 1986) and, as noted above, access to the study area can be difficult. Therefore, by necessity, the temporal and spatial resolution of this method is variable and tends to be poor.

Schwarzacher (1959) and Untersteiner (1968) studied the salinity distribution and desalination processes in multi-year ice. Based on their own experiments and work by Nakawo and Sinha (1981), Cox and Weeks (1975, 1988) developed a numerical model of the salinity profile of first-year sea ice that is valid before the flushing of the ice during summer melt. However, their model fails to capture the high-frequency variations in the salinity profile due to rapid changes in meteorological conditions (Cox and Weeks, 1988). Furthermore, it tends to underestimate the salinity of thin ice and overestimate the salinity of thick ice (Cox and Weeks, 1988), and it does not describe the large horizontal variations observed in the field (Bennington, 1967; Tucker et al., 1984). In this paper, we

present a non-destructive method suitable for obtaining long time series of bulk salinity and relative brine volume at centimeter resolution in naturally growing sea ice. This work builds on studies by Vant (1976), Vant et al. (1978), and Morey et al. (1984), who conducted thorough theoretical and experimental investigations of the dielectric properties of sea ice. Vant (1976) also provides an exhaustive overview of previous work. Arcone et al. (1986) showed that the complex dielectric properties of natural sea ice change with time, opening the possibility to track changes in bulk salinity and ice microstructure. A non-destructive method to track changes in ice salinity was recently presented by Notz et al. (2005), based on changes in impedance between platinum wires frozen into the ice. Here, we employ a commercially available capacitance probe to derive complex dielectric permittivity data of the bulk sea ice at 50 MHz. The dependence of the real part of the complex dielectric permittivity on brine volume fraction and brine salinity is then utilized to derive the bulk salinity of the ice, in conjunction with in situ temperature measurements.

1.3 Methodology

1.3.1 Complex dielectric permittivity of sea ice

Naturally occurring sea ice is a complex dielectric mixture whose three main components are pure ice, liquid brine, and air bubbles. At temperatures below -22.9 °C, precipitated

salts also become a significant component, and under certain conditions particle inclusions and microorganisms can form part of the mixture.

Each of the components of sea ice, or similar mixtures, has its own distinctive dielectric properties. Their relative concentrations and distribution determine the dielectric properties of the sea ice, or mixture (Stogryn, 1987; Chelidze and Gueguen, 1999; Chelidze et al., 1999; Fabbri et al., 2006). For this study we do not consider surface effects of polarization or clustering of components (Chelidze and Gueguen, 1999; Chelidze et al., 1999; Moore and Maeno, 1993). Clustering, or the development of discrete continuous paths of the conductive component, occurs near the percolation threshold only; and we as yet lack information about the ice-brine interface in the brine inclusions.

In this paper we will limit our study to the complex dielectric permittivity of columnar first-year sea ice, which makes up most of the interior of the ice, below or near the percolation threshold, 50–70‰ (Weeks and Ackley, 1986; Golden et al., 1998). The percolation threshold occurs when the relative brine volume becomes so large that the discrete brine inclusions start to connect and form networks, enabling gravitational drainage. If the salinity of the ice is 5 ‰, which is a valid assumption for the interior of Arctic first-year ice, the percolation threshold is reached around a temperature of -5 °C (Golden et al., 1998). Thus, we can assume that we have a mixture of pure ice and brine only, with the brine occurring in discrete pockets within the ice matrix. We leave to future studies frazil and platelet ice with their irregular crystal structure and brine

inclusion morphology, as well as ice close to its melting point and multi-year ice with their complex mixtures, including air bubbles. The complex dielectric permittivity, $\varepsilon=\varepsilon'-i\varepsilon''$, of both of these materials is described by the Debye (1929) equation:

$$\varepsilon = \varepsilon_{\infty} + \frac{\varepsilon_{l} - \varepsilon_{\infty}}{1 + i\omega\tau} - \frac{i\sigma}{\varepsilon_{0}\omega} \tag{1.1}$$

where:

ε = Complex frequency-dependent dielectric permittivity

ε_l = Static complex dielectric permittivity of the material

ε_∞ = High frequency complex dielectric permittivity of the material

ε_0 = Complex dielectric permittivity of free space

ω = Angular frequency of the signal

τ = Relaxation time of the material

σ = Ionic conductivity of the material

$i = (-1)^{1/2}$

The studies by Morey et al. (1984) and Arcone et al. (1986) showed that ε' depends mostly on the relative brine volume V_b/V, and less on the brine inclusion geometry. Converesly, the imaginary part of the complex dielectric permittivity, ε'', is more dependent on the geometry of the inclusions, and less on the on the relative brine volume (Morey et al., 1984). However, Kovacs and Morey (1979), and Morey et al. (1984)

showed that crystal orientation does affect ε', with a reduction for a configuration with the electrical field vector parallel to the c-axis of the ice crystals, as discussed in more detail below.

1.3.2 Instrumentation

We chose to use the Stevens Water Monitoring Systems Hydraprobe for this study. It was originally developed by Campbell (1988; 1990) for non-destructive, in-situ measurements of soil moisture. The rugged design and lack of need for maintenance makes it ideal for semi-permanent emplacement, and for long-term measurements in frozen materials (Romanovsky and Yoshikawa, personal communication, 2000; Yoshikawa et al., 2004).

The Hydraprobe is a coaxial probe with a central tine surrounded by three equally spaced outer tines, all made out of stainless steel. The three outer tines are held at ground potential, and a voltage is applied to the central tine at 50 MHz frequency, resulting in a circularly polarized wave (see Table 1.1 for a list of relevant probe parameters; Campbell, 1990; Stevens Water Monitoring Systems, 1994). The probe head also contains a thermistor for temperature measurements. Since the thermistor is located inside the probe, it measures, strictly speaking, the temperature of the probe, but the probe has for the most part the same temperature as the surrounding ice. The error for the temperature given in Table 1.1 is for the entire temperature range at which the probe is designed to operate. Comparison with arrays of thermistors, deployed in conjunction with

the Hydraprobe arrays (see below), indicate an uncertainty in the temperature of ~ 0.2°C over the temperature intervals studied here.

Brine volumes larger than 300 ‰ (Stevens Water Monitoring Systems, 1994), and large vertical variations in brine volume over a few centimeters in the skeletal layer of the bottommost few centimeters of the ice, for instance, result in large errors that preclude further data analysis.

The output data is in the form of four voltages: V1-4, where V1-V3 give the capacitive and conductive response of the material, and V4 gives the temperature. The raw voltages were converted using a program supplied by Stevens Water Monitoring Systems.

In the field, the probes were connected to a Campbell CR10X datalogger. The measurements were made using a single ended measurement over a +/2.5V interval. The signal was integrated over 2.72 mS. The measurements were stored in Campbell Scientific SM716 storage modules, which were regularly changed, and data downloaded to PC laptops. The setup was powered by a 12V marine battery, with the connection only switched on during measurements.

In the field we mounted the Hydraprobes on 2-inch diameter PVC half pipes, which were deployed by drilling through thin, growing ice, with the tines protruding from the convex side. The ice was then allowed to embed the probes naturally. Examination of ice thin-sections cut around probes revealed no major deviations from ice microstructure of standard congelation ice, i.e., a columnar ice crystal structure with subparallel, vertically oriented layers of brine between submillimeter ice lamellae. Visual inspection also

indicates that ice crystals do not nucleate on the tines ahead of the advancing lower boundary of the ice (Cotter and Miner, personal communication, 2005; Notz et al., 2005).

The datalogger and storage module were deployed in insulated boxes on the ice, together with the batteries to keep them protected from the harsh environment and direct sunlight, and were recording data every 10 to 30 minutes.

Together with the arrays of capacitance probes in McMurdo and Barrow, two arrays of thermistors were deployed to measure the temperature profile of the ice. One array on each site was operated by the authors and the other was operated by colleagues from Victoria University, New Zealand. Their vertical spacing was 0.1 m (further details can be found in Pringle et al., in press).

At the time of deployment, at the time of probe extraction, and in between, 0.1 m diameter ice cores were obtained through the entire thickness of the ice for stratigraphic analysis. The temperature of the cores was measured, and 0.1 m sections of the cores were melted for determination of salinity by using a YSI 30 conductivity probe (measurement error <0.02 or <1% of the bulk salinity, whichever is larger).

In both McMurdo and Barrow the experiment sites were chosen on undeformed land-fast ice, without leads or ridges nearby.

1.3.3 Laboratory and field experiments

1.3.3.1 Measurements in landfast sea ice in McMurdo Sound, Antarctica, July 10 – November 11, 2002

An array of four Hydraprobes was deployed at 77.73°S 166.44°E on July 10, 2002 in the first-year landfast ice of McMurdo Sound, northwest of the Erebus ice tongue. The probes were deployed at depths of 0.85 m, 1.05 m, 1.25 m, and 1.45 m. One thermistor array was deployed 3.4 m away, and the other 100 m away. The site was tended to by members of the overwintering crew at the New Zealand Scott Base. Ice thickness at deployment was approximately 1.2 m. The arrays were retrieved on November 11 by the authors and colleagues from Victoria University, New Zealand. A core drilled at the site at this time indicated an ice thickness of 2.3 meters.

Readings were taken every 30 minutes. For this analysis we only consider data from the bottommost two of the four probes. The two topmost probes were deployed within the drill hole, as the ice thickness was greater at deployment than anticipated, and the ice within the borehole is not considered representative of natural conditions at the site. The bottommost probes were encased by the growing ice.

Air temperatures were obtained from Automatic Weather Station Pegasus North (77.958°S 166.5°E), operated by the Space Science and Engineering Center, University of Wisconsin-Madison, USA.

1.3.3.2. Measurements in landfast sea ice off Barrow, Alaska, February 2 – June 4, 2003

An array of three Hydraprobes was deployed in the Chukchi Sea landfast ice, 156.67°W, 71.34°N, on February 2, 2003 in ice of 0.7 m thickness. The probes were deployed at depths of 0.4 m, 0.6 m, and 0.8 m below the upper surface of the ice. As in the McMurdo experiment, the thickness of the ice was underestimated, and only data from the lowermost probe is analyzed in this paper. The array was recovered on June 7 from ice with a thickness of 1.29 m. One thermistor array was deployed 1 m away from the dielectric probe array, and the other 50 m away.

Three cores were taken during the course of the experiment: one during deployment on February 2, one on April 8, 50 meters away from the site but in ice of comparable thickness and microstructure, and one on June 4 when recovering the array.

Air temperature data have been obtained with a shielded thermometer mounted at 2 m height at the same site (data provided by D. K. Perovich, Cold Regions Research and Engineering Laboratory, Hanover, NH).

1.3.3.3. Outdoor ice tank experiment, Fairbanks, Alaska, February 8 – April 20, 2003

To compare the field results with an experiment under controlled conditions, probes were deployed in a 1.5 m^3 meter outdoor tank at the Geophysical Institute of the University of

Alaska Fairbanks. The tank was filled with spring water and Instant Ocean artificial sea salt from Aquarium Systems to simulate seawater with salinity of 32 ‰.

The tank was fitted with both a thermostat and heater to regulate ice growth. A pressure relief valve system connected to a glycol reservoir prevented pressure build-up in the tank, which could potentially push brine upwards through the ice. A low-speed circulation pump to mix the water was also fitted to the tank, but it malfunctioned at an unknown time during the experiment. Ice thickness was measured twice daily with a weighted wire gauge frozen into the ice. On April 15, when the last core was obtained, the ice thickness exceeded 0.45 m.

Four Hydraprobes were fitted in a plastic mesh: two at 0.03 m, and two at 0.19 m depth in the water. We have used data from only one of the lowermost probes for this analysis, due to the large variations in temperature and the later radiative heating of the ice that complicated analysis of this data from the topmost probes, and due to malfunction of the other probe at 0.19 m depth in the ice.

Air temperature data, as provided by the National Weather Service, comes from the meteorological station at Fairbanks International Airport, situated 5 km from the experiment site.

1.4 Results and analysis

1.4.1 Field data

1.4.1.1 McMurdo Sound

The output from the Hydraprobes, together with air temperature data, is shown in Fig. 1.1. Because of the extreme conditions in McMurdo Sound, some data were lost due to equipment malfunctions. Here, we only consider data between August 21 and October 9. Both the timeseries of the temperature and of ε' are comparatively stable. This is due to the fact that the probes were deployed at a depth to which very little shortwave radiation penetrated, reducing the effect of the daily surface temperature variation. We see slight increases in the values of both real valued complex dielectric permittivity and ice temperature around August 28 (day 240) and September 25 (day 268), in response to atmospheric warming in the preceding days.

The salinity profile from the retrieved core is shown in Fig. 1.2. Comparison with other cores taken at the same time in the McMurdo Sound area and other data from the Antarctic (Eicken, 1992) indicates that the salinity profile is representative of Antarctic undeformed first-year ice. At a depth of 1.47 m in the core, approximately the depth of the lowermost probe, a layer of milky, less-transparent ice was observed, something occasionally associated with columnar ice growth in McMurdo Sound (Gow et al., 1998).

1.4.1.2 Barrow

The entire time series of the real part of the complex dielectric permittivity, ice, and air temperature data, from the time at which the probe was frozen into the ice cover on February 27 up to the retrieval of the array on June 7, is shown in Fig. 1.3. We have truncated the time series at $\varepsilon' = 20$, so as to better be able to distinguish features in the data after freeze-in of the probe. On June 2 (day 153) there is a sharp increase in ε', followed by a decrease. This coincides with the time when the ice is close to melting temperature throughout its thickness, around the period when we would expect substantial brine motion or even flushing, and corresponding changes in ice salinity.

The salinity data from the three cores retrieved during the experiment are shown in Fig. 1.4. The winter cores exhibit a typical C-shaped profile with high surface salinities and mostly stable salinities in the interior ice. After onset of surface melt, the surface 0.2 m of the ice desalinated rapidly due to meltwater flushing. A vertical thin-section was produced from a core retrieved on February 24 2003, 50 m distant, but from the same depth and type of ice as that embedding the probe. The ice consisted of large columnar crystals with horizontal c-axis alignment. Brine inclusions consisted of vertically oriented parallel layers and tubes of brine.

1.4.1.3 Ice tank experiment

The air temperature, ice temperature, and ε' as measured during the ice tank experiments are shown in Fig. 1.5. Due to technical difficulties two periods of data were lost: February 21 to March 2 and March 18 to 23.

The probe was emplaced only 0.19 m below the upper surface of the ice, so the daily air temperature variations had an effect on both the ice temperature and on the complex dielectric permittivity, as measured by the probe. During the course of the experiment, diurnal temperature cycles and radiative heating of the probe (and the ice) became increasingly prominent.

Salinity data from the four cores retrieved during the course of the experiment are shown in Fig. 1.6. The ice cover was kept free of snow during the entire experiment. From the beginning of April onwards the upper surface of the ice started to ablate. Later, with increasing temperatures, between April 5 and April 9 (days 94 and 99) a layer of meltwater formed on the upper surface of the ice. Even though the temperatures at a depth of 0.19 m were still comparatively low, the values of ε' started to increase on April 9 (day 99), perhaps because of solar heating and local warming around the tines.

The cores here show rapid desalination, which can be expected with the large temperature gradients in the thin ice, and evidence of flushing in the upper 0.2 meters of the core of April 15.

1.4.2 Deriving the bulk salinity of the ice from complex dielectric permittivity measurements

1.4.2.1 Apparent aspect ratio of brine inclusions in sea ice

The purpose of this study is to develop a method for determining the bulk salinity by measuring the complex dielectric permittivity and temperature of the ice. The complex dielectric permittivity of sea ice is not directly dependent on the bulk salinity, but rather on the relative brine volume of the ice, and the geometry of the brine inclusions.

In columnar ice, the brine inclusions take the form of ellipsoids below and around the percolation threshold, with the major axis vertical, or close to vertical (Assur, 1960; Cole and Shapiro, 1998; Eicken et al., 2000; Light et al., 2003). Addison (1970) showed that ε' has a dependency on the aspect ratio between the major and minor axes of the ellipsoidal brine inclusions, with brine inclusions with large aspect ratios contributing relatively more to the total ε' than brine inclusions with smaller aspect ratios. Vant (1976), Golden and Ackley (1980), Morey et al., (1984), and Arcone et al., (1986) adapt the dielectric mixture model developed by Tinga et al. (1973) to model the complex dielectric behavior of sea ice. Tinga's model assumes vertically aligned, ellipsoidal brine inclusions enclosed in a medium with complex dielectric permittivity ε_{MIX}, which is the complex dielectric permittivity of sea ice in this case.

This model is highly simplified, since in reality the dimensions of the brine inclusions vary from submillimeters to several millimeters in the vertical, and the inclusions are not

symmetrical in the horizontal plane (Perovich and Gow, 1996; Eicken et al., 2000; Light et al., 2003). Arcone et al. (1986) stressed the need for a complex dielectric permittivity mixture model based on actual dimensions of the brine inclusions, and not only their aspect ratios.

Cole and Shapiro (1998) estimated an average aspect ratio of the brine inclusions in Arctic ice of ~ 9 in their sample from the ice interior. Their sample was taken from a depth of 0.8 meters in the landfast ice in the Chukchi Sea outside Barrow, Alaska. Light et al. (2003) showed that around 50% of all brine inclusions in their three samples from the columnar interior of Arctic sea ice had aspect ratios between 10 and 20, and that these values changed little between -15 and -5°C, but increased as the ice approaches melting temperature.

Tinga's model requires an average value of the aspect ratios of the brine inclusions. Still, using Tinga's relation will allow a first assessment of linkages between our permittivity measurements and in-situ salinities. To be able to use Tinga's relation we must first, however, cast it in terms of the brine volume and bulk salinity of the ice:

$$\frac{\varepsilon_{AV}-\varepsilon_1}{\varepsilon_1}=\frac{V_2}{V_1}*\frac{\varepsilon_2-\varepsilon_1}{\left[-(V_2/V_1)n*(\varepsilon_2-\varepsilon_1)+n(\varepsilon_2-\varepsilon_1)+\varepsilon_1\right]} \quad (1.2)$$

where:

V_2 = brine volume

V_1 = pure ice volume

n = depolarization coefficient which is dependent on the eccentricity of the ellipsoids

ε_1 = complex dielectric permittivity of pure ice

ε_2 = complex dielectric permittivity of brine

ε_{AV} = complex dielectric permittivity of the sea ice mixture

The full method of calculating the temperature-dependent complex dielectric permittivity of pure ice and brine, ε_1 and ε_2, is given in Vant (1976).

The dimensions of the brine inclusions cannot be considered small in comparison to the probe dimensions (Stevens Water Monitoring Systems, 1994; Campbell, 1988; Cole and Shapiro, 1998; Eicken et al., 2000; Light et al., 2003), therefore the ice will be assumed as anisotropic relative to the probe. The resulting value of ε_{MIX} measured by the probe is given by (Vant 1976):

$$\varepsilon'_{MIX} = \frac{\varepsilon'_{AV(a)}}{2} + \frac{\varepsilon'_{AV(b)}}{2} \tag{1.3}$$

where:

$\varepsilon'_{AV(a)}$ = the real part of the complex dielectric permittivity with the electrical field parallel to the major axis of the brine inclusion

$\varepsilon'_{AV(b)}$ = the real part of the complex dielectric permittivity with the electrical field parallel to the minor axis of the brine inclusion

The results of these calculations can be seen in Fig. 1.7. We have plotted ε' (dots) from the three experiments against the corresponding temperatures. Bounding the experimental values are theoretical values calculated using Equations 1.2 and 1.3 (dashed lines with theoretical values in parenthesis). It is clear that for all the experiments, the apparent aspect ratio experienced by the probes correlates well with the aspect ratios measured by Cole and Shapiro (1998) and by Light et al. (2003). The aspect ratios measured by Eicken et al., (2000) are somewhat smaller. Furthermore, both the Barrow (B) and ice tank experiment (C) data sets show strong increases in the apparent aspect ratio with the ice temperature close to the melting or freezing of the ice, which is also in agreement with the observations by Light et al. (2003). Above the percolation threshold more and more networks of linked brine inclusions are formed, and the morphology of the brine inclusions become more complex than is covered by our model.

1.4.2.2 Establishing the relation between the real part of the complex dielectric permittivity and the bulk salinity of sea ice

As stated above, ε' is mainly dependent on the relative brine volume of the ice, V_b/V. Cox and Weeks (1983) and Leppäranta and Manninen (1988) developed a set of equations describing V_b/V as a function of the bulk salinity and temperature of the ice based on the phase relations in thermodynamic equilibrium:

$$\frac{V_b}{V} = \frac{\rho S}{F_1(T) - \rho S F_2(T)} \tag{1.4}$$

where:

ρ = the temperature dependent density of pure ice

S = the bulk salinity of the ice

T = temperature in °C

$F_{1,2}(T)$ = empirical polynomial functions of temperature based on phase relations in the ice

With ice temperature measured by the probes and the brine volume fraction estimated from the complex dielectric permittivity measurements, we can estimate the bulk salinity of the ice.

Fig. 1.8 shows the relative brine volume V_b/V as a function of ε' for all four probes. In the graph we have excluded data points where the temperature was higher than –2°C, since interpretation of this data is complicated by probes extending into the skeletal layer, or into rotten ice, as well as potential solar heating. The chemical composition of the brine inclusions close to the melting point of ice is also uncertain. For reasons of clarity we have chosen to plot only every 20^{th} data point, even though we have used the entire data set for our calculations. For the Barrow measurements we have also chosen to plot the periods from February 24 (day 55) to April 8 (day 98), and April 8 to June 7 (day 158) separately. We labeled these periods 'cooling' and 'warming'. The relative brine volumes have been calculated using Equation 4 with the measured salinity data from the cores, assuming constant desalination rates between measurements. This is a valid assumption, supported by the research by Nakawo and Sinha (1981) and Cox and Weeks (1986), considering that the bulk salinity changes very little between the core measurements at the depths of the probes.

It is clear from the graph that the data points from Barrow, the ice tank experiment, and from the probe at 1.45 m depth interval at McMurdo all follow a linear relation between ε' and V_b/V. The reason why the data from the probe at depth 1.25 m in the McMurdo experiment deviates from this line, and is hence excluded, is covered in more detail below.

From Fig. 1.8 we can develop a linear regression formula that describes the relation between V_b/V and ε':

$$\frac{V_b}{V} = a + b\varepsilon' \tag{1.5}$$

where:

a = -0.0582

b = 0.0113

With $R^2 = 0.9748$

Equation 1.5 can be fitted to an inversion of Equation 4 to obtain an expression that links the bulk salinity directly with ε', see Equation 1.6:

$$S = \frac{1}{\rho} * \frac{(a + b\varepsilon')F_1(T)}{1 + (a + b\varepsilon') * F_2(T)} \tag{1.6}$$

where:

ρ = the temperature dependent density of pure ice

S = the bulk salinity of the ice

T = temperature in °C

$F_{1,2}(T)$ = empirical polynomial functions of temperature based on phase relations in the ice

a,b = the conastants in the kinear regression formula that describes the relation between V_b/V and ε'

Comparing with previous experimental results (Morey et al., 1984; Arcone et al., 1986), this relation should be valid for relative brine volumes at least up to 100 ‰, with error limits of less than 25% above the percolation threshold. We can suspect that above relative brine volumes of 100 ‰ the morphology of the brine inclusions have changed so much that the simple assumptions of discrete brine inclusions no longer hold.

We know from thin sections that the Hydraprobes were deployed in columnar ice in Barrow and in the ice tank. If there is a current present, the c-axis of the columnar ice crystals will align parallel to it (Weeks and Gow, 1978). This was observed at Barrow with the current parallel to the shore (Cole and Shapiro, 1998), and the probe tines parallel to the c-axis of the columnar ice. In the absence of a current in the ice-tank experiment no preferred c-axis alignment of the columnar ice crystals was observed. Both Kovacs and Morey (1979), and Morey et al. (1984) showed that if the electrical field is parallel to the preferred c-axis alignment of the columnar ice crystals, it will result in a decrease in ε'.

The expected ice-growth at depth in McMurdo is aggregation of so-called platelet ice at the bottom of the ice sheet (Jeffries et al., 1993; Gow et al., 1998; Jones and Hill, 2001; Smith et al., 2001). A vertical thin-section from 1.1-1.2 m depth at the study site in McMurdo Sound suggests that at this depth interval ice crystals are starting to deviate from the typical columnar structure, with tilted platelets and finer grained ice. Lacking data for the depth interval of 1.2-1.3 meters depth we can assume that the ice has a less well organized structure at this depth, with further platelet accumulations. This, along with higher connectivity between pores, and a reduced degree of anisotropy for such ice,

explains much of the observed deviation from the regression curve in Fig. 1.8, and the lower values of bounds of the apparent aspect ratio observed in Fig. 1.7 A (Golden, personal communication, 2005).

The unexpectedly large values of the bounds of the apparent aspect ratio of the deeper probe could be explained by the presence of the observed milky layer in the core at that depth. Jeffries et al. (1993) and Gow et al. (1998) did report observing layers of columnar ice interspaced with layers of platelet ice in McMurdo Sound. This could explain the differences in apparent aspect ratio observed by the two probes in the McMurdo experiment.

1.4.2.3 Salinity change in the landfast sea ice at Barrow, Alaska, 2003

We will now investigate how useful the Hydraprobes are in measuring the salinity changes in sea ice. We chose the data from the Barrow experiment for this, since it is the most complete time series of temperature and dielectric permittivity that we have collected, and because we have good sets of supplementary data to compare the results.

Time series of the relative brine volume and bulk salinity (Fig. 1.9 A and B) of the ice at Barrow have been arrived at by using Equations 4 and 6, in conjunction with the data provided by the Hydraprobe. Fig. 1.9 C, showing the daily change in salinity as derived from the salinity data in Fig. 1.9 B, indicates several events during which the bulk salinity of the ice surrounding the Hydraprobe changes rapidly. Fig. 1.9 D shows the

temperatures recorded by the Hydraprobe and by the thermistor in the adjacent string deployed at about the same depth as the Hydraprobe. The temperature records are similar but not identical, this is partly due to the fact that the Hydraprobe records the temperature inside the probe casing, while the independent thermistor measures the temperature of the ice itself. Also, the two instruments measure the temperatures at two different locations in the ice. Niedrauer and Martin (1979) showed that the isotherms in sea ice are not horizontal, but vary with the thickness of the ice. The thickness of the ice can vary even over short distances (personal observation by the authors at Barrow, 2003).

Using the independent data provided on the temperature evolution of the ice cover by the thermistor string deployed in conjunction with the Hydraprobe array, we will discuss the salinity evolution and potential brine movement in more detail below.

The thermal evolution of the ice cover is apparent from the contour diagram of daily ice temperatures at depth levels spaced 0.1 m apart (Fig. 1.10 A). Three distinct temperature regimes can be discerned in the ice: (1) rapidly growing ice with a drop in ice temperatures, prior to about day 80 (March 21); (2) a cold stable period, between days 80 and 118 (March 21 – April 28), with ice temperatures at the probe's depth level below –5 °C; and (3) early spring warming after day 118 (April 28) to the end of observations in early June, with temperatures between –5 and –2 °C at the probe's depth level.

However, it is the connectivity between the brine inclusions that controls the rate of gravity drainage, which is the main desalination mechanism in cold sea ice (Cox and Weeks, 1975). Based on measured salinity profiles, we have estimated the desalination rate from which salinity profiles could be reconstructed at different time points. From this

data, in turn, time series of brine volume evolution were derived (Fig. 1.10 B). In Fig. 1.10 C, one can discern three episodes of apparent brine movement that are above the error limit: around day 65 (March 6), around days 90 – 95 (March 31 – April 5), and around days 115 – 121, (April 25 – May 1).

The third episode takes place in the warming ice temperature regime. In Fig. 1.9 A-C we see rapid increases in both relative brine volume and bulk salinity, followed by similar decreases. The temperature recorded by the independent thermistor shows a similar decrease followed by an increase (this temperature variation is barely recorded by the thermistor in the Hydraprobe, since it is not sensitive enough). Hudier et al. (1995) recorded a similar thermal event in sea ice, attributing the temperature change to cold dense brine flushing down through porous ice, and then being replaced by seawater from below the lower boundary of the ice. Neither the downward flushing brine nor the seawater that replaces it is in thermal or haline equilibrium with the surrounding ice. Therefore the ice will first cool as the oversaturated brine dissolves the ice, and then warm as latent heat is released by the freezing of the seawater (Worster and Wettlaufer, 1997). Both the brine and seawater will increase the salinity of the already desalinated ice. This effect appears to be temporary however. We do see from the cores (Fig. 1.4) that despite desalination of the upper surface of the ice, the bulk salinity of the interior changes very little. The substantial drop in surface salinities does not occur until meltwater flushing starts in late May (Eicken et al., 2002). It is apparent that this event is not an overturning in a single brine channel, since it is recorded not only by the Hydraprobe and the adjacent thermistor string, but also by the thermistor string deployed

50 m distant (Pringle et al., submitted). This event also coincides with the period when the ice above the probe becomes permeable to brine movement (Golden et al., 1998) as shown in Fig 10 B.

The first of the episodes, around day 65 (March 6), takes place during a period of rapidly growing ice while the probe is still embedded in very porous ice close to the ice-ocean interface. This event is only recorded by the Hydraprobe, not by the independent thermistor (Fig. 1.9 D). This, and the relatively low relative brine volume of the ice above the probe, would lead us to suspect that it is a convective plume of seawater penetrating up into the ice from beneath the ice-ocean interface. Such plumes were observed by Niedrauer and Martin (1979) in laboratory experiments of simulated sea ice.

The second episode takes place between days 90 and 95 (March 31 – April 5), during a period of stable, low ice temperatures, when the overall salinity of the ice is fairly stable as well (Fig. 1.9 A). From Figs. 3 A and B it is apparent that this increase in ε' coincides with an increase in temperature. This correlation suggests that the salinity excursion is merely an artifact, resulting from the assumption of a constant desalination rate, which can lead to artificial changes in the derived salinity during periods of stable ice salinity. In contrast, during the second half of the time series, the reduction in bulk ice salinity appears to be captured well, despite increasing temperatures.

1.4.2.4 Sources of error

There are two sources of error in the experiment: errors stemming from the uncertainties in the measurements of the bulk salinity, and instrument errors. The error limits for the Hydraprobe are given in Table 1. The probe measures average temperature and •' over its entire volume. However, using the measured values of air temperature and ice thickness, we arrived at an average temperature gradient in the ice of less than 0.2°K/cm for all the experiments. Then, by using the estimated average bulk salinities from the ice cores, we calculated that the contribution to the error in relative brine volume from the instrumental uncertainty is less than 5%.

This indicates that the main source of error for this experiment is the uncertainty in the original bulk salinity measurements that form the basis of the regression developed in Fig. 1.8. First, the bulk salinity measurements are averaged over a volume of ice larger than and not directly adjacent to the volume sampled by the probes. Field studies (Bennington, 1967; Tucker et al., 1984) indicate that horizontal variations can be significant, up to 3 ‰ over distances of 0.25 meters. However, parallel cores taken in the homogeneous fast ice at Barrow typically vary by much less than 1‰ at any given depth level. This justifies an estimated error of 0.5‰ in the salinity measurement (Tucker et al., 1984). Secondly, we assume a constant desalination rate between subsequent cores. Our own results and earlier studies by Notz et al. (2005) in growing ice indicate that the brine movements are not continuous, but rather episodical. Studies by Eide and Martin (1975) and Freitag and Eicken (2003) indicate that the main brine movement in sea ice after

initial growth takes place within secondary brine inclusion features, for instance, when the initial pores link up to form tubes and channels. For a further investigation of these convective overturnings in sea ice we refer to Eicken et al. (in preparation).

Thus, there is an error associated with the salinity measurements that enters into Equation 4. Based on salinity data from ice cores, it appears that the salinities in the Barrow experiment might be overestimated by as much as 20% for the period after initial embedding of the probe in the interior of the ice, and before April 8. There is a similar maximum overestimation of 20% of the bulk salinity in the tank experiment in the period leading up to April 15.

Fig. 1.7 indicates that the apparent aspect ratios seen by the probes stay constant for temperatures throughout much of the studied temperature interval. We can therefore assume that the brine inclusion morphology does not change significantly within the temperature and complex dielectric permittivity intervals this study focuses on; this assumption is in agreement with the studies by Eicken et al., (2000) and Light et al., (2003). However, further work is needed to validate this assumption and investigate the impact of potential changes in pore morphology on dielectric permittivity measurements.

To calculate the error in the estimate of the bulk salinity, we will have to use the standard formula for error propagation twice: once for Equation 4 with the error in temperature and the error in the bulk salinity measurement, and then for Equation 6 with the resulting error in brine volume and the error in temperature. The resulting error in bulk salinity, as measured by the Hydraprobe under the conditions outlined above, is

below 15% below the percolation threshold, increasing to 25% as the ice gets close to the melting/freezing temperature.

1.5 Conclusions

We have presented in this paper results from three separate experiments, in which we have deployed commercially available capacitance probes in natural, undeformed first-year sea ice in the field, and under experimental conditions. We have shown that, within the limitations stated for these experiments, it is possible to measure both the absolute values of the bulk salinity and changes in bulk salinity with large temporal and spatial resolutions, and within a reasonable error limit. This is particularly interesting during periods when rapid desalination of the ice is known to occur, e.g. just after initial freezing and during ice melt, even though, at present, the error limit of our measurements during these periods can be large.

We have concentrated on the real part of the dielectric permittivity ε' in this study. While ε' mainly depends on the relative brine volume and temperature of the ice, the distribution, size, morphology and orientation of the brine inclusions also affect it. These factors increase the overall measurement error, ideally requiring independent data on ice microstructure. At the same time, however, this allows for indirect assessments of changes in microstructure during warming or cooling of the ice, in particular with a set of probes frozen in with different tine/field orientations. The probes also measure the

imaginary part of the complex dielectric permittivity, which is more sensitive to the morphology of the brine inclusions. This suggests that with additional information on bulk salinity and ice microstructure from cores (Eicken et al., 2000; Light et al., 2003), the error limits of the bulk salinity measurements can be significantly reduced. At the same time, this offers the possibility to monitor brine pocket evolution using the same techniques described in this paper.

Our results compare well with theory as expressed in the model developed by Tinga et al. (1973). This could be partly due to the brine being mostly concentrated in brine inclusions with large aspect ratios (Light et al., 2003), which provide a large relative contribution to the real value of the complex dielectric permittivity (Addison, 1970). The circular geometry of the probes also makes the absolute orientation of the brine inclusions unimportant in these experiments because of the microstructure of the ice investigated. However, more sophisticated electromagnetic property models may help improve significantly the salinity and brine volume estimates from inversion of permittivity data (Golden, personal communication, 2005), especially for ice which is above the percolation threshold, where more complex brine inclusion morphology is expected, or in frazil or platelet ice, which exhibits a smaller degree of anisotropy than the columnar ice investigated here. This would enable the probes to be used at high temperatures when flushing events take place, and when increases in porosity make the ice more laterally permeable (Cottier et al., 1999; Freitag and Eicken, 2003). Covering the tines with tubing will reduce the probe's sensitivity to contiguous brine

concentrations, which would also increase the usefulness of the probe in highly porous ice (Yoshikawa et al., 2004).

The method employed by Notz et al. (2005) in deriving ice salinity from indirect measurements is more sensitive, has better spatial resolution, and works well in the skeletal layer in the ice. However, it only provides the relative concentrations of solid and brine fraction, but does not provide information on the morphology of the brine inclusions. The method described in this paper can be used to model the morphology of the brine inclusions because of the geometry of the Hydraprobe, as described above. Furthermore, our method utilizes relatively cheap, robust, and commercially available probes, which might make it preferable to incorporate them into larger scale studies, such as in the deployment of drifting buoy packages. A further improvement of the capacitance method would include measurements of the capacitance between sensors deployed in parallel vertical boreholes or narrow slits in the ice. Such deployment would be particularly advantageous if it could be achieved without disturbing the ice and without the need for the ice matrix to freeze around the sensors.

1.6 Figures

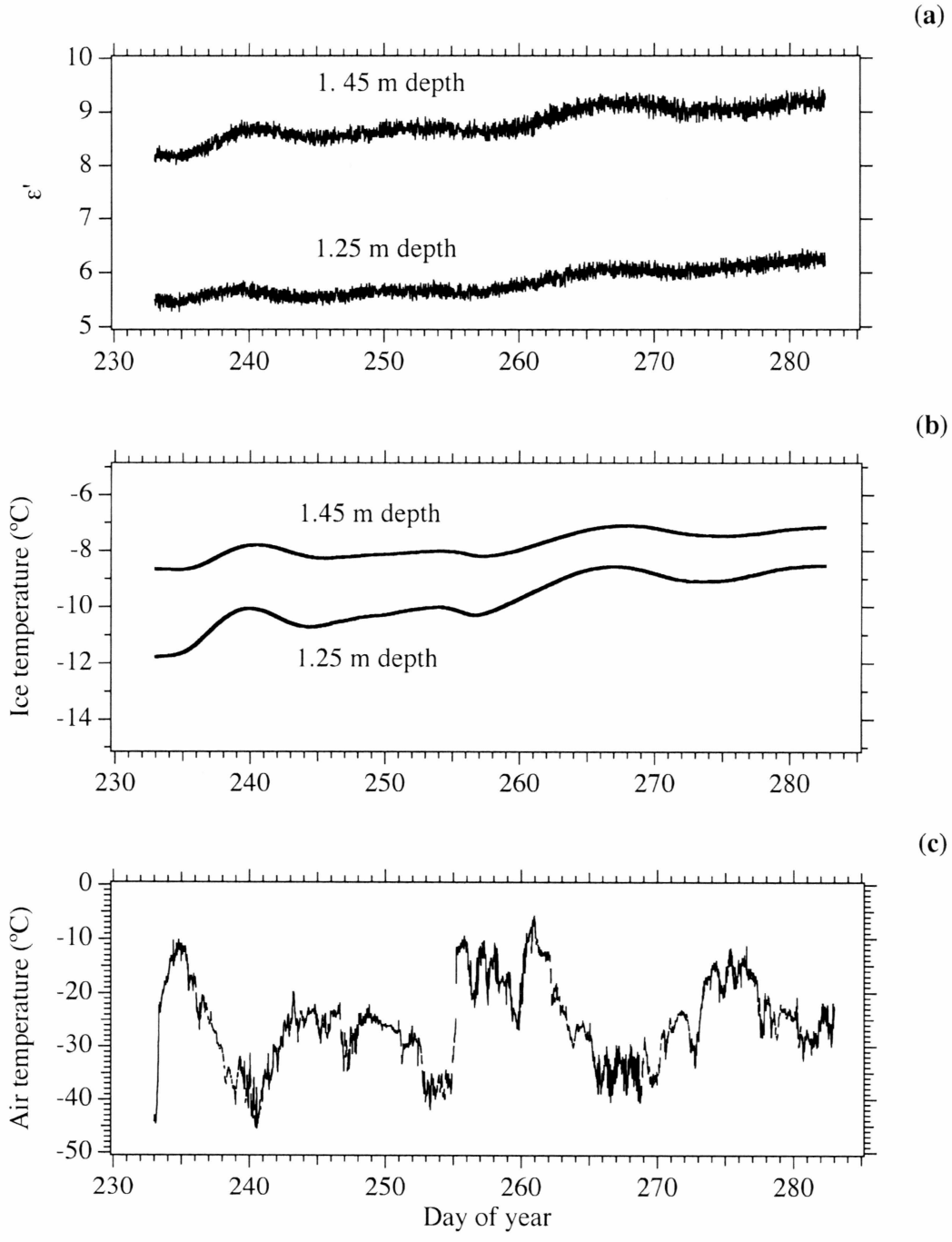
(a)
1. 45 m depth
1.25 m depth
ε'
(b)
1.45 m depth
1.25 m depth
Ice temperature (°C)
(c)
Air temperature (°C)
Day of year

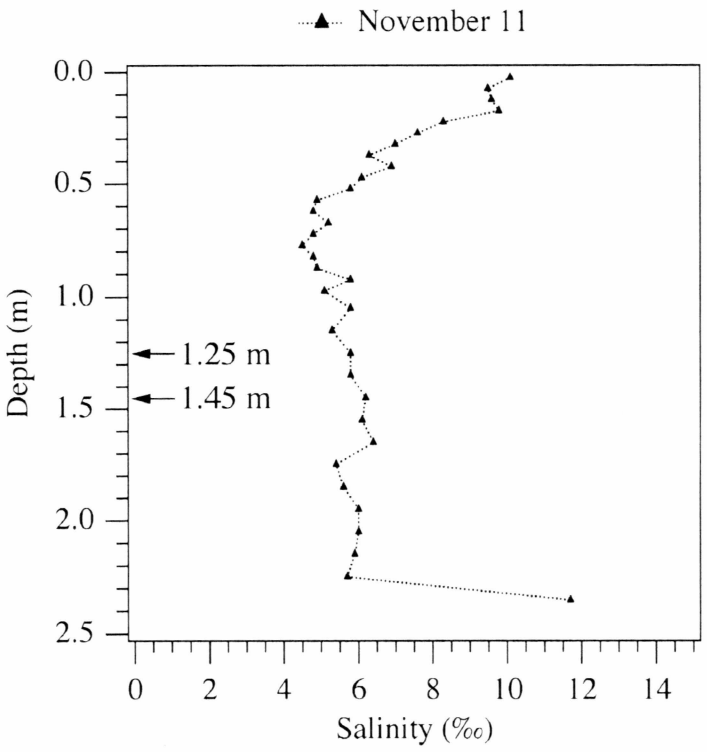

Fig. 1.2. Salinity profile from the core retrieved November 11, 2002. 1.2 meters away from the Hydraprobe array in McMurdo Sound. The arrows indicate the approximate depths of the probes.

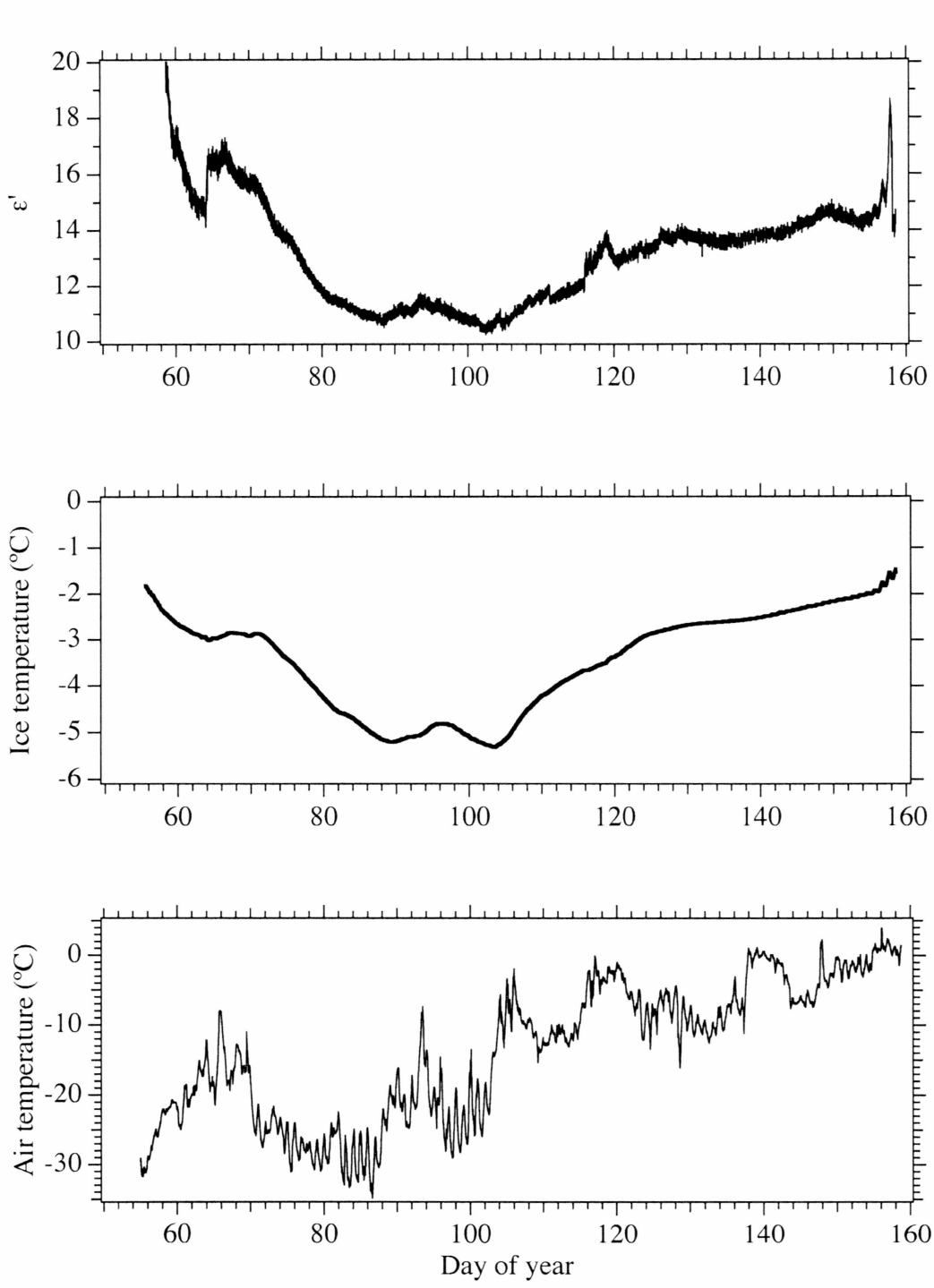
A
20
18
16
14
12
10
ε'
60
80
100
120
140
160
B
0
-1
-2
-3
-4
-5
-6
Ice temperature (°C)
60
80
100
120
140
160
C
0
-10
-20
-30
Air temperature (°C)
60
80
100
120
140
160
Day of year

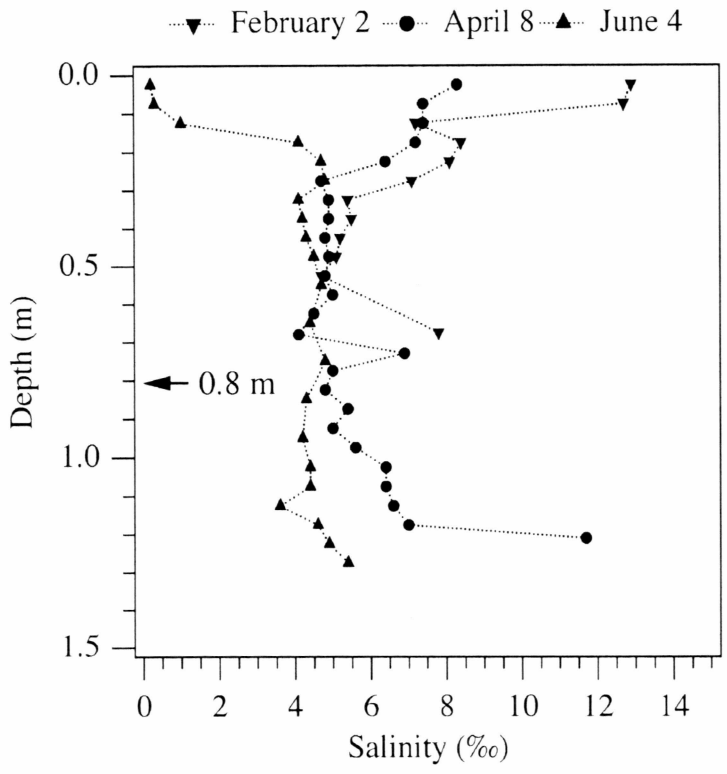

Fig. 1.4. Salinity profiles from the cores retrieved at or near the measurement site off Barrow, 2003, where the Hydraprobe array was deployed. The arrow indicates the approximate depth of the probe.

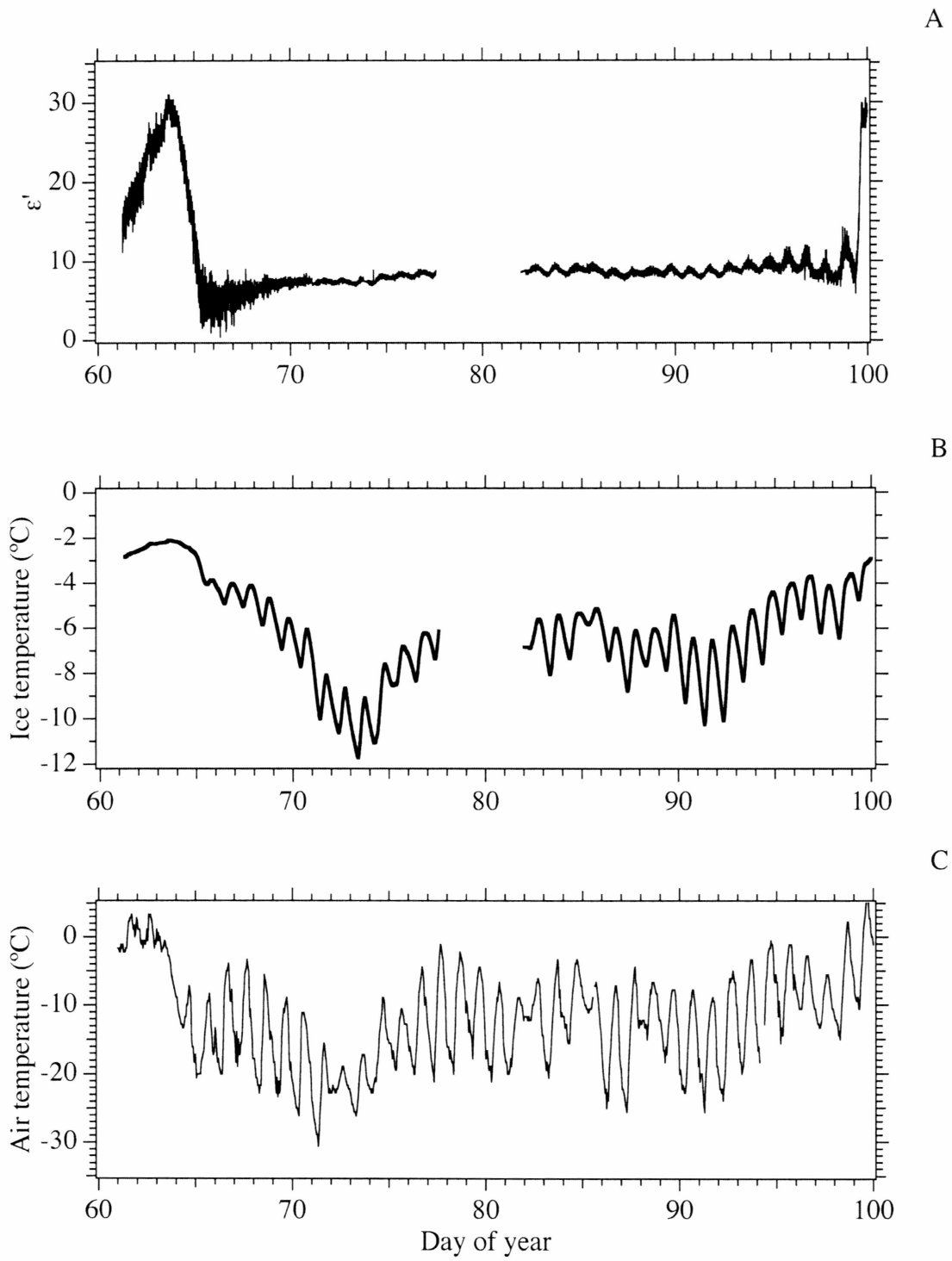
A
30
20
10
0
ε'
60
70
80
90
100
B
0
-2
-4
-6
-8
-10
-12
Ice temperature (°C)
60
70
80
90
100
C
0
-10
-20
-30
Air temperature (°C)
60
70
80
90
100
Day of year

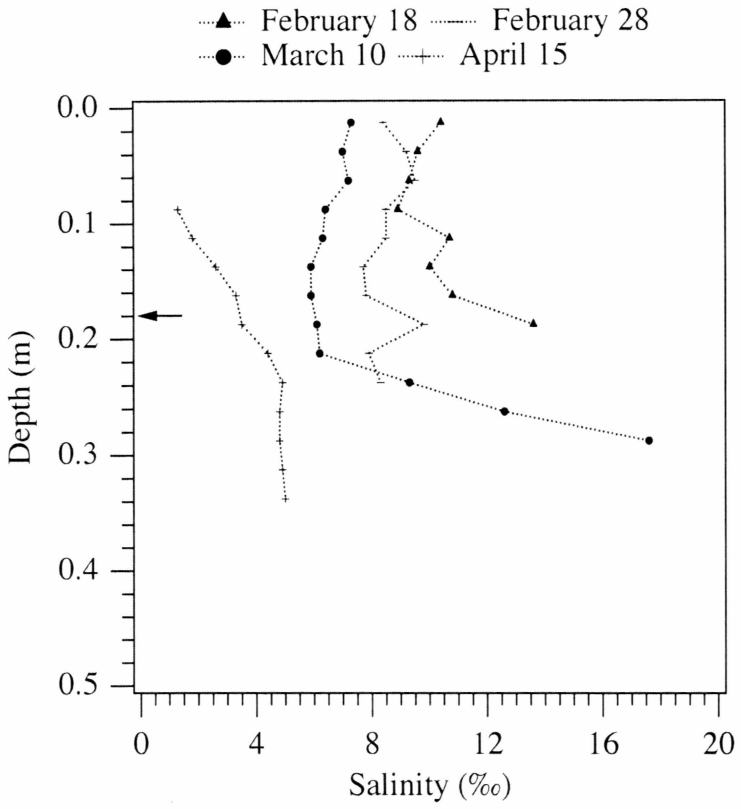

Fig. 1.6. Salinity profiles of the cores in the ice tank experiment. The arrow indicates the depth of the probe. The core retrieved on April 15 did not reach the bottom of the ice.

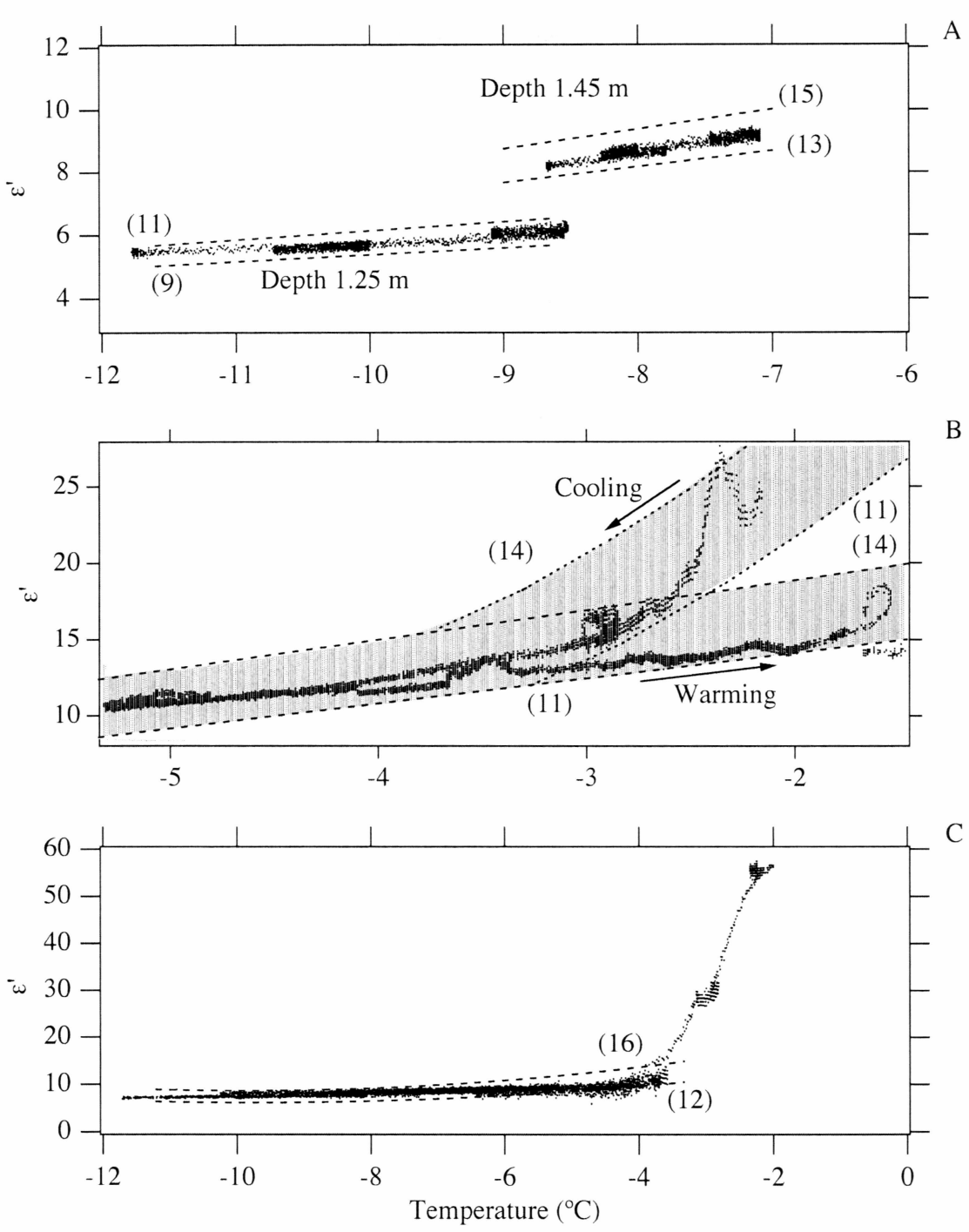
A
12
10
8
6
4
ε'
Depth 1.45 m
(15)
(13)
(11)
(9)
Depth 1.25 m
-12
-11
-10
-9
-8
-7
-6
B
25
20
15
10
ε'
Cooling
(14)
(11)
(14)
(11)
Warming
-5
-4
-3
-2
C
60
50
40
30
20
10
0
ε'
(16)
(12)
-12
-10
-8
-6
-4
-2
0
Temperature (°C)

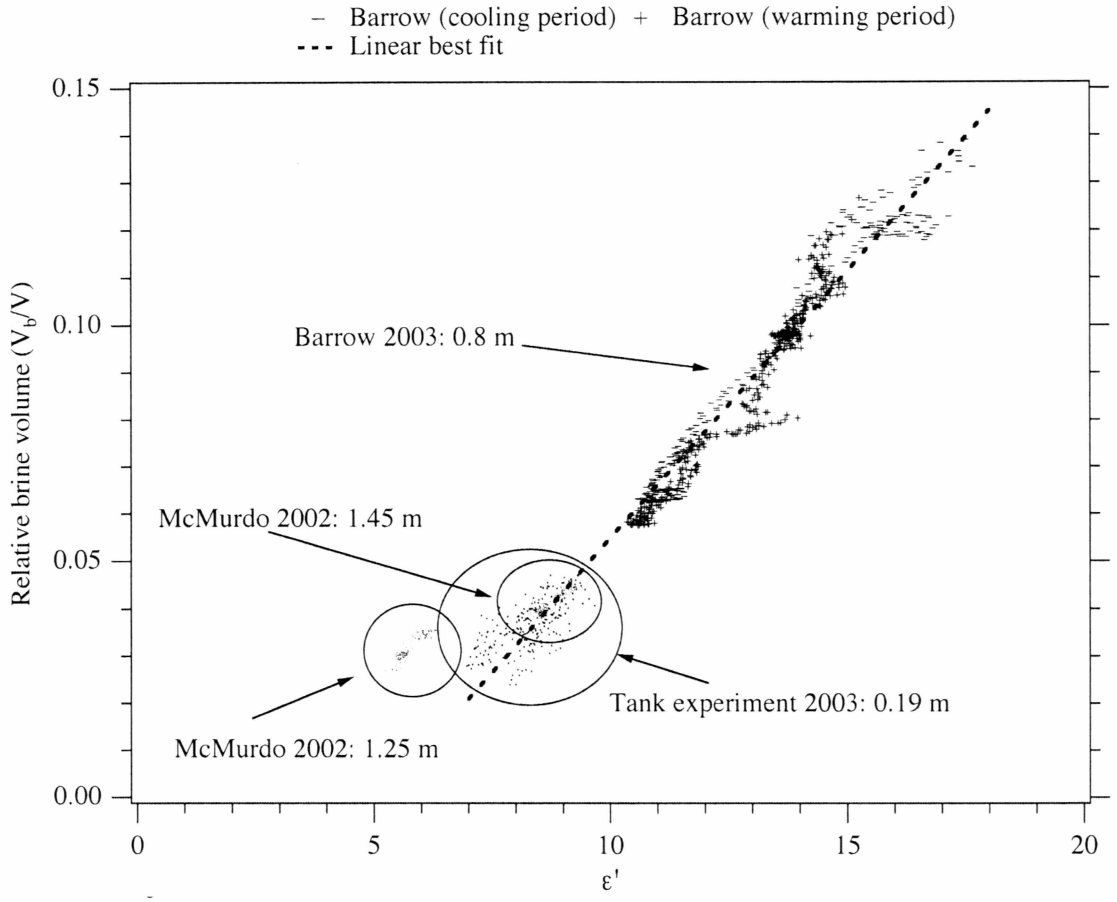

Fig. 1.8. The relative brine volume V_b/V as a function of the real part of the complex permittivity for all the probes. Data for temperatures above -2°C are excluded from the calculations. The straight line is a linear best fit to all the data, excluding the probe from McMurdo Sound deployed at depth of 1.25 meters.

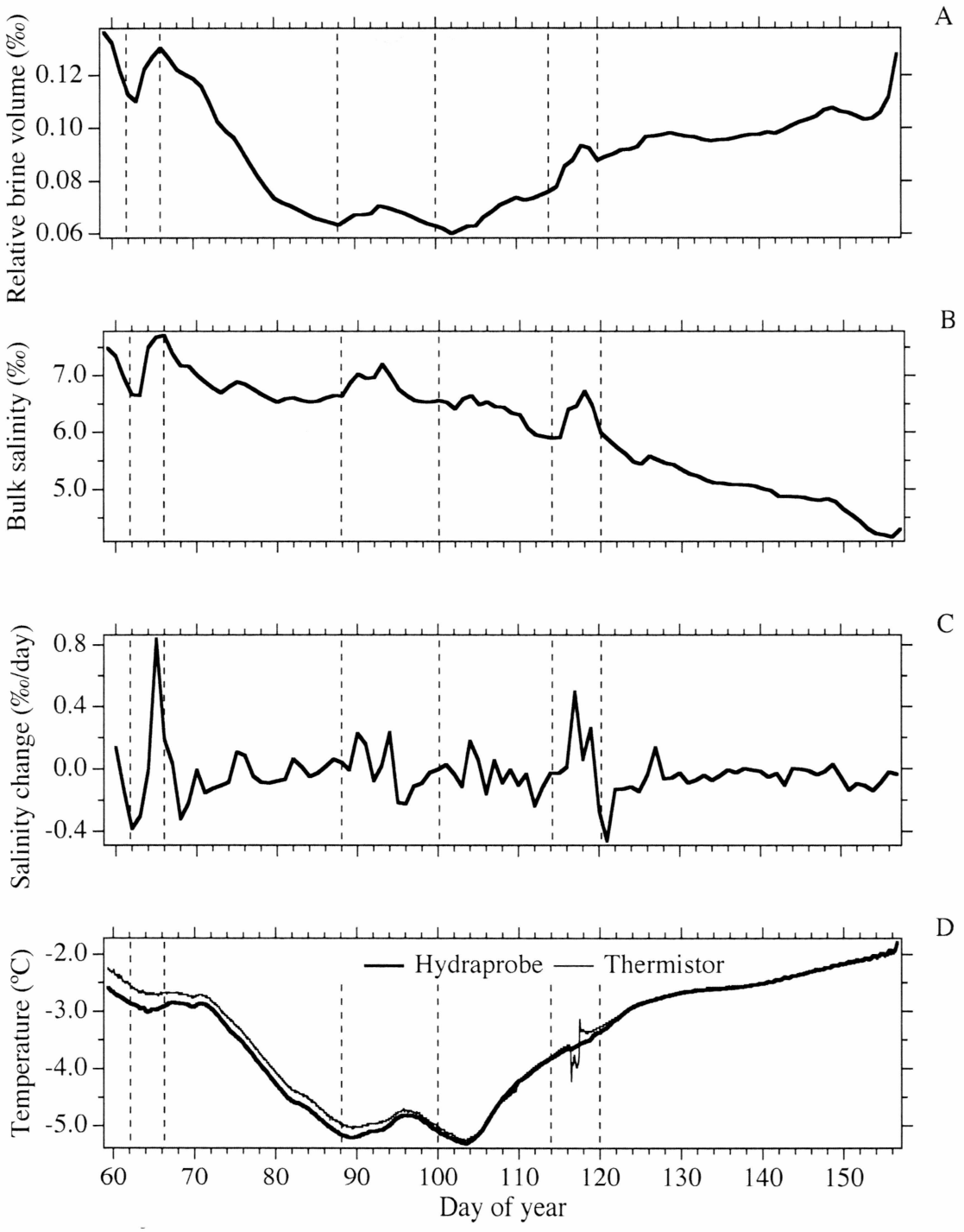
A
Relative brine volume (‰)
0.12
0.10
0.08
0.06
B
Bulk salinity (‰)
7.0
6.0
5.0
C
Salinity change (‰/day)
0.8
0.4
0.0
-0.4
D
Temperature (°C)
-2.0
-3.0
-4.0
-5.0
Hydraprobe
Thermistor
60
70
80
90
100
110
120
130
140
150
Day of year

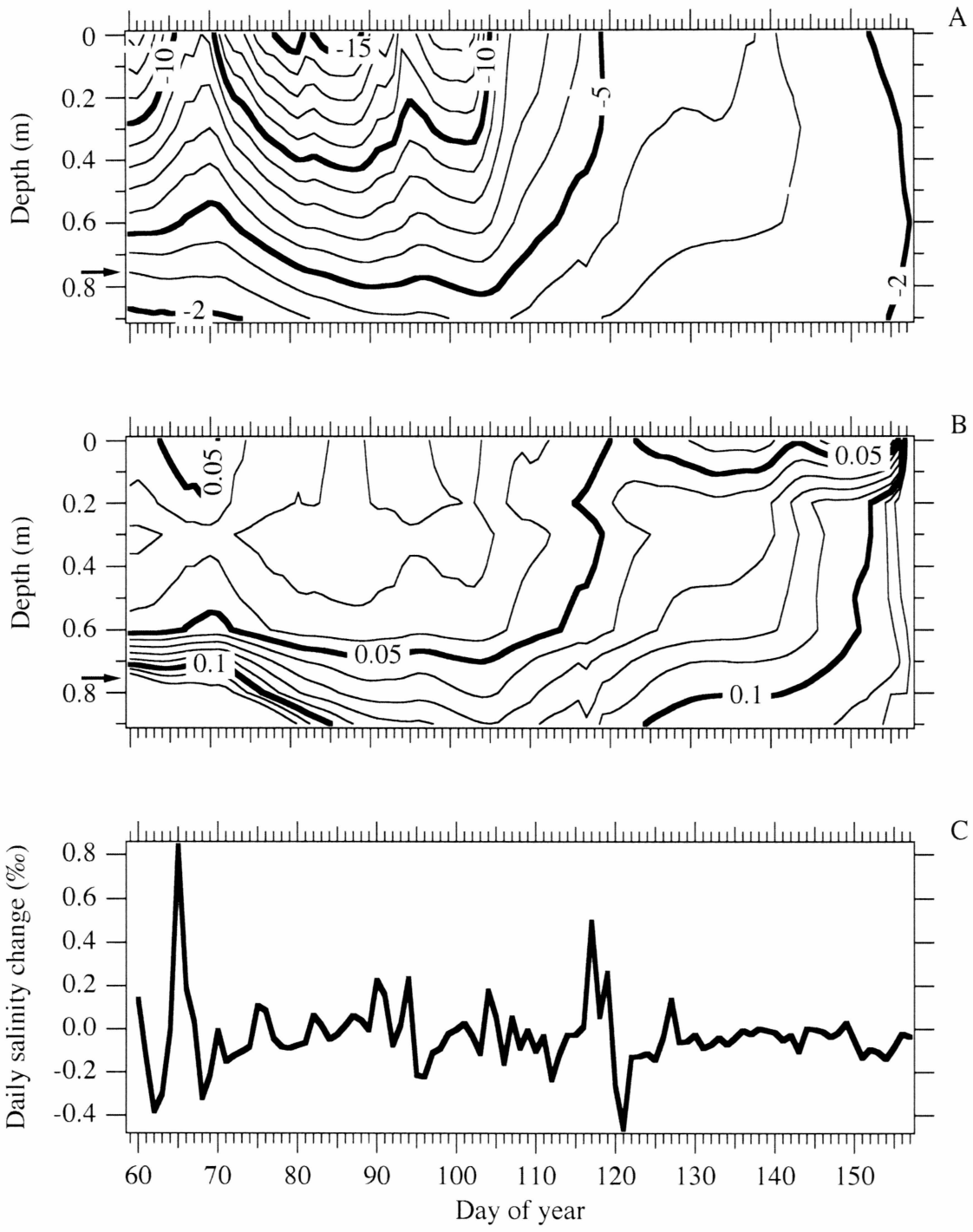
A
Depth (m)
0
0.2
0.4
0.6
0.8
-10
-15
-10
-5
-2
-2
B
Depth (m)
0.05
0.05
0.05
0.1
0.1
C
Daily salinity change (‰)
0.8
0.6
0.4
0.2
0.0
-0.2
-0.4
60
70
80
90
100
110
120
130
140
150
Day of year

1.7 Tables

Table 1.1. Technical specifications of the Hydraprobe capacitance probe.

Tine length (mm)	57
Tine diameter (mm)	4
Probe radius (mm)	15
Sensing volume (mm^2)	13000
Dielectric measurement error	±0.2
Specified temperature measurement error (°K)*	±0.6

*The error in temperature ±0.6 °K is for the entire operating range of -15°C - 65°C. For the temperature range in our experiments the error was considerably smaller.

1.8 References

Addison, J. R., 1970. Electrical relaxation in saline ice. Journal of Applied Physics, 41(1): 54-63

Arcone, S. A., Gow, A. J. and McGrew, S., 1986. Structure and dielectric properties at 4.8 and 9.6 GHz of saline ice. Journal of Geophyiscal Research, 91(C12): 14281-14303

Assur, A., 1960. Compostition of sea ice and its tensile strength. CRREL Report , 44. U. S. Army Cold Regions Research and Engineering Laboratory, Hanover, NH

Bennington, K. O., 1967. Desalination features in natural sea ice. Journal of Glaciology, 6(48): 845-857

Bitz, C. M. and Lipscomb, W. H., 1999. An energy-conserving thermodynamic model of sea ice. Journal of Geophyiscal Research, 104(C7): 15669-15677

Campbell, J. E., 1988. Dielectric properties of moist soils at rf and microwave frequencies. Ph.D. Thesis, Dartmouh College, Hanover, NH

Campbell, J. E., 1990. Dielectric properties and influence of conductivity in soils at one to fifty megahertz. Soil Science of America Journal, 54(2): 332-341

Chelidze, T. L. and Gueguen, Y., 1999. Electrical spectroscopy of porous rocks: a review. I. Theoretical models. Geophysical Journal International, 137(1): 1-15

Chelidze, T. L., Gueguen, Y. and Ruffet, C., 1999. Electrical spectroscopy of porous rocks: a review. II. Experimental results and interpretation. Geophysical Journal International, 137(1): 16-34

Cole, D. M. and Shapiro, L. H., 1998. Observations of brine drainage networks and microstructure of first-year sea ice. Journal of Geophyiscal Research, 103(C10): 21739-21750

Comiso, J. C., 2003. Large-scale characterisics and variability of the global sea ice cover. In: Eds. D. N Thomas and G. S. Dieckmann, Sea ice - an introduction to its physics, chemistry, biology and geology. Blackwell, Oxford, UK, pp. 112-143

Cottier, F., Eicken, H. and Wadhams, P., 1999. Linkages between salinity and brine channel distribution in young sea ice. Journal of Geophysical Research, 104(C7): 15859-15871

Cox, G. F. N. and Weeks, W. F., 1975. Brine drainage and initial salt entrapment in sodium chloride ice. CRREL Report, 354. U. S. Army Cold Regions Research and Engineering Laboratory, Hanover, NH

Cox, G. F. N. and Weeks, W. F., 1983. Equations for determining the gas and brine volumes in sea-ice samples. Journal of Glaciology, 29(102): 306-316

Cox, G. F. N. and Weeks, W. F., 1986. Changes in the salinity and porosity of sea-ice samples during shipping and storage. Journal of Glaciology, 32(112): 371-375

Cox, G. F. N. and Weeks, W. F., 1988. Numerical simulations of the profile properties of undeformed first-year sea ice during the growth season. Journal of Geophyiscal Research, 93(C10): 12449-12460

Debye, P., 1929. Polar molecules. Dover Publications Inc., New York

Dieckmann, G. S. and Hellmer H. H., 2003. The importance of sea ice: an overview. In: Eds. D. N Thomas and G. S. Dieckmann, Sea ice - an introduction to its physics, chemistry, biology and geology. Blackwell, Oxford, UK, pp. 1-22

Eicken, H., 1992. Salinity profiles of Antarctic sea ice: field data and results. Journal of Geophyiscal Research, 97(C10): 15545-15557

Eicken, H., 2003. From the microscopic to the macroscopic, to the regional scale: growth, microstructure and properties of sea ice. In: Eds. D. N Thomas and G. S. Dieckmann, Sea ice - an introduction to its physics, chemistry, biology and geology. Blackwell, Oxford, UK, pp. 22-82

Eicken, H., Bock, C., Wittig, R., Miller, H. and Poertner, H.-O., 2000. Magnetic resonance imaging of sea ice pore fluids: methods and thermal evolution of pore microstructure. Cold Regions Science and Technology, 31: 207-225

Eicken H., Krouse, H. R., Kadko, D. and Perovich, D. K., 2002. Tracer studies of pathways and rates of meltwater transport through Arctic summer sea ice. Journal of Geophysical Research, 107(10): 8046, DOI 10.1029/2000JC000583

Eicken, H., Cole, D. M. Backstrom, L. G. E., Pringle, D. Shapiro, L. H. and Trodahl, J., in preparation. Permeability-porosity relationships and convective heat transfer in first-year Arctic sea ice. Journal of Geophysical Resesearch

Eide, L. I. and Martin, S., 1975. The formation of brine drainage features in young sea ice. Journal of Glaciology, 14(70): 137-154

Fabbri, A., Fen-Chong, T. and Coussy, O., 2006. Dielecric capacity, liquid water content, and pore structure of thawing-freezing materials. Cold Regions Science and Technology 44(1): 52-66

Freitag, J. and Eicken, H., 2003. Meltwater circulation and permeability of Arctic summer ice derived from hydrological field experiments. Journal of Glaciology, 49(166): 349-358

Golden, K. M. and Ackley, S. F., 1980. Modeling of anisotropic electromagnetic reflection from sea ice. CRREL Report, 80-23, U. S. Army Cold Regions Research and Engineering Laboratory, Hanover, NH

Golden, K. M., Ackley, S. F. and Lytle, V. I., 1998. The percolation phase transition in sea ice. Science, 282: 2238-2241

Gow, A. J., Ackley, S. F., Govoni, J. W., and Weeks, W. F., 1998. Physical and structural properties of land-fast sea ice in McMurdo Sound, Antarctica. In: Ed. M. O. Jeffries, Antarctic sea ice:physical processes, interactions and variability. Antarctic research series. American Geophysical Union, Washington, DC, pp. 74355-74374

Hudier, E. J.-J., Ingram, R. G., and Shirasawa, K., 1995. Upward flushing of sea water through first year ice. Atmosphere-Ocean, 33: 569-580

Jeffries, M. O., Weeks, W. F., Shaw, R. and Morris, K., 1993. Structural characteristics of congelation and platelet ice and their role in the development of Antarctic land-fast sea ice. Journal of Glaciology, 39(132): 223-238

Jones, S. J. and Hill, B. T., 2001. Structure of sea ice in McMurdo Sound, Antarctica. Annals of Glaciology, 33: 5-11

Kovacs, A. and Morey R. M., 1979. Anisotropic properties of sea ice in the 50- to 150-MHz range. Journal of Geophyiscal Research, 84(C9): 5749-5759

Leppäranta, M. and Manninen, T., 1988. The brine and gas content of sea ice with attention to low salinites and high temperatures. Finnish Institute of Marine Research Internal Report, 88-2. Helsinki, Finland

Light, B., Maykut, G. A. and Grenfell, T. C., 2003. Effects of temperature on the microstructure of first-year Arctic sea ice. Journal of Geophyiscal Research, 108(C2): 3051, DOI 10. 1029/2001JC000887

Maykut, G. A., 1986. The surface heat and mass balance. In: Ed. N. Untersteiner, The geophysics of sea ice. Plenum Press, New York, pp. 395-463

Moore, J. C. and Maeno, N., 1993. Dielectric properties of frozen clay and silt soils. Cold Regions Science and Technology, 21: 265-273

Morey, R. M., Kovacs, A. and Cox, G. F. N., 1984. Electromagnetic properties of sea ice. CRREL Report, 80-20, U. S. Army Cold Regions Research and Engineering Laboratory, Hanover, NH

Nakawo, M. and Sinha, N. K., 1981. Growth rate and salinity profile of first-year sea ice in the high Arctic. Journal of Glaciology, 27(96): 315-330

Niedrauer, T. M., and Martin, S., 1979. An experimental study of brine drainage and convection in young sea ice. Journal of Geophysical Research, 84(C3): 1176-1186

Notz, D., Wettlaufer, J. S. and Worster, M. G., 2005. A non-destructive method for measuring the salinity and solid fraction of growing sea ice in situ. Journal of Glaciology, 51(172): 159-166

Perovich, D. K. and Gow, A. J., 1996. A quantitative description of sea ice inclusions. Journal of Geophysical Research, 101(C8): 18327-18343

Pounder, E. R., 1965. The physics of ice. Pergamon Press, Oxford, UK

Pringle, D. J., Eicken, H., Trodahl, H.J. and Backstrom, L, in press. Thermal conductivity of land-fast Antarctic and Arctic sea ice. Journal of Geophysical Research

Schwarzacher, W., 1959. Pack ice studies in the Arctic Ocean. Journal of Geophyiscal Research, 64(12): 2357-2367

Smith, I. J., Langhorne, P. J., Haskell, T. G., Trodahl, H. J., Frew, R. and Vennel, M. R., 2001. Platelet ice and the land-fast sea ice of McMurdo Sound, Antarctica. Annals of Glaciology. 33: 21-27

Stevens Water Monitoring Systems. 1994. Hydra soil moisture probe user's manual version 1.2 with floppy disk. Stevens Water Monitoring Systems, Beaverton, OR

Stogryn, A., 1987. An analysis of the tensor dielectric constant of sea ice at microwave frequencies. IEEE Transactions on Geoscience and Remote Sensing, GE-25(2): 147-158

Tinga, W. R., Voss, W. A. G. and Blossey, D. F., 1973. Generalized approach to multiphaze dielectric mixture theory. Journal of Applied Physics, 44(9): 3897-3902

Tucker, W. B., Gow, A. J. and Richter, J. A., 1984. On small-scale horizontal variations of salinity in first-year sea ice. Journal of Geophyiscal Research, 89(C4): 6505-6514

Untersteiner, N., 1968. Natural desalination and equilibrium salinity profile for perennial sea ice. Journal of Geophyiscal Research, 73(4): 1251-1257

Vant, M. R., 1976. A combined empirical and theoretical study of the dielectric properties of sea ice over the frequency range. Ph.D. Thesis, Carleton University, Ottawa, Canada

Vant, M. R., Ramseier, R. O. and Makios, V., 1978. The complex-dielectric constant at frequencies in the range 0.1-40GHz. Journal of Applied Physics, 49(3): 4712-4717

Weeks, W. F. and Ackley, S. F. 1986. The growth, structure and properties of sea ice. In: Ed. N. Untersteiner, The geophysics of sea ice. Plenum Press, New York, pp. 9-164

Weeks, W. F. and Gow, A. J., 1978. Crystal alignment in the fast ice of Arctic Alaska. CRREL Report, 79-22. U. S. Army Cold Regions Research and Engineering Laboratory, Hanover, NH

Worster, M. G. and Wettlaufer, J.S., 1997. Natural convection, solute trapping, and channel formation during solidification of saltwater. Journal of Physical Chemistry B, 101(32): 6132-6136

Yoshikawa, K., Overduin, P.P. and Harden, J. W., 2004. Moisture content measurements of moss (Sphagnum spp.) using commercial sensors. Permafrost and Periglacial processes, 15: 309-318

Chapter 2 Analysis of brine movement in first-year sea ice based on a case study of temperature and dielectric permittivity data

2.1 Abstract

For four seasons between 1999/2000 and 2002/2003 arrays of thermistors were operated together with mass balance sites on the level landfast first-year sea ice in the Chukchi Sea outside Barrow, Alaska. During the season 2002/2003, instruments measuring the complex dielectric permittivity of the ice were also deployed, together with a separate thermistor array. Thermistor and dielectric permittivity data clearly indicate percolation events through their effects on ice temperature and porosity.

Records from the instrument arrays together with mass balance and bulk salinity data from cores are in this paper used to further analyze these brine percolation events. The focus will be on an event observed by three separate instrument arrays on April 27, 2003.

Despite the comparably long duration and magnitude of the event, it did not significantly modify the conductive heat flow in the ice. Moreover, and despite several years of observation, only one substantial large-scale drainage event was observed. Therefore, the conclusion is that the observed brine movement events do not contribute significantly to the overall heat budget of the ice.

2.2 Introduction

2.2.1 Aims

The primary purpose of this study is to investigate the percolation of brine within the ice using arrays of thermistors and capacitance probes. These instruments measure changes in the temperature and dielectric permittivity of the ice. These variations indicate changes in the structure and porosity of the ice.

During the period of research several events occurred where either the temperature or the dielectric permittivity of the ice, or both, changed. The rapidity of these events implies that they are due to changes of brine volume in the ice.

The secondary purpose of this study was to study how much, if at all, these events contributed to the energy budget of the ice. This was achieved by estimating the magnitude of the convective heat transfer associated with the events.

2.2.2 Theory

As sea ice grows, some liquid in the form of discrete brine pockets is trapped within the ice matrix. This salt water is trapped either between the ice crystals, or grains, or inside the crystals between the parallel platelets that follow the basal plane orientation of the crystal (see Fig. 2.1). The upper ice layer typically consists of randomly oriented granular (frazil) ice crystals. Deeper in the ice, where the ice crystals are typically columnar in shape, the c-axes of the individual crystals may exhibit parallel alignment, especially if there is a dominant current, as is the case in Barrow (Cole and Shapiro, 1998).

Bennington (1967) was the first to observe that brine inside the ice occurs in either

discrete brine pockets or in refrozen brine channels, and he labeled them primary and secondary brine features, respectively. Wakatsuchi and Saito (1985) and Wakatsuchi and Kawamura (1987) analyzed the distribution of the channels, as well as their tendency to form in columnar ice, but not in frazil ice. However, Bennington (1967), Lake and Lewis (1970), Eide and Martin (1975), Tucker et al. (1984), Wakatsuchi and Saito (1985), Wakatsuchi and Kawamura (1987), Cole and Shapiro (1998), Cottier et al. (1999) and Miner (2007) all observe that brine channels are a phenomenon of ice growth, and that brine channels in the interior of the ice are frozen and filled with fine-grained ice crystals, (see Fig 2.2). Cottier et al. (1999) also associated the brine channels with higher bulk salinity than the surrounding ice.

Cole and Shapiro (1998), and Miner (personal communication, 2006) have observed that even though the spatial distribution and diameters of the refrozen brine channels remain approximately constant throughout the interior of the ice few, if any, individual brine channels extend uninterrupted throughout the interior of the ice at low (below -5°C) temperatures during much of ice-growth season.

Weeks and Ackley (1986), Golden et al. (1998), and Golden (2001), showed that the brine pockets start to connect and form networks when the relative brine volume of the ice is higher than 50-70‰. This brine volume corresponds roughly to a temperature of -5°C and a salinity of 5‰ in what Golden (2001) calls the "rule of fives." The connectivity of brine pockets is not solely vertical, but also lateral. This lateral connectivity can be used to explain the redistribution of brine and homogenization of the bulk salinity of ice that has been "warmed," (observed by Cottier et al., 1999).

Since the upper layers of the ice have a high bulk salinity (Malmgren, 1927), radiative heating of the ice during spring will create a hydraulic head (Niedrauer and Martin, 1979) in the freeboard layer, which will then drive gravity drainage of the brine if there are

connected brine networks in the underlying ice reaching through the entire ice thickness.

Eide and Martin (1975), Niedrauer and Martin (1979), and Worster and Wettlaufer (1997), describe the process of gravity-driven brine movement and the thermal effects of cold, dense brine flowing into ice that is warmer than the equilibrium temperature for the brine.

The thermistors capture the temperature variations and the Hydraprobe dielectric permittivity sensor measures changes in the complex dielectric permittivity as the displaced brine melts the surrounding ice. Since the instruments are deployed in-situ in natural sea ice, it is possible to capture these events as they occur, and at the same time attempt to estimate their effect on the overall heat budget of the ice.

2.3 Study area and instrumentation

Every year, the Sea Ice Group at the University of Alaska Fairbanks Geophysical Institute operates a mass-balance site in the landfast, undeformed first-year sea ice in the Chukchi Sea outside Barrow, Alaska, (see Fig 2.3).

Throughout the seasons mass balance and ice core data were obtained (see Table 2.1 for freeboard and snow depth data from the different seasons). The freeboard and snow depths were measured using tape at the time of retrieval. Note that the cores for the 2000/2001 season were not retrieved at the mass balance or thermistor array sites, but rather at sites just off the beach at the Ukpeagvik Inupiat Corporation-Naval Arctic Research Laboratory (UIC-NARL). The salinity data obtained from the cores, using the method described in Backstrom and Eicken (2006), is shown in Figure 2.4.
During the seasons 1999/2000 to 2002/2003 additional instruments were deployed, see Table 2.2. For technical details and methodology see Backstrom and Eicken (2006) and

Pringle et al. (in press).

Figure 2.5 shows the temperature profiles in the ice for all four years. Note that only the months March, April, and May are shown, since those are the months where brine movement events have been observed (Eicken et al., in preparation).

The horizontal thermistor arrays deployed during the 1999/2000 season consisted of three U-shaped frames deployed at depths of 0.6 m, 0.85 m, and 1.1 m. Ten thermistors were attached to each frame, with three thermistors each to the sides, and four on the base of the U. Their horizontal spacing was 0.05 m.

2.4. Results and analysis

2.4.1. Analysis of individual events

Figure 2.6 shows examples of sudden temperature changes recorded by the thermistor arrays during the 1999/2000 season. Figures 2.6 A and B show events registered by the lateral thermistor array. Only the thermistors registering events are shown. There are three notable circumstances regarding these recordings:

-It is always the same thermistors that registered the percolation events.
-Theses events are only recorded by one thermistor per depth level – no other thermistor at the same depth registers any temperature change, despite a lateral separation of only 0.05 meters.
-The thermistors at the different depths that record the temperature changes are not aligned vertically; rather, they are aligned at an angle of ~45°.

Figure 2.6 C shows two events that were only recorded by a vertical thermistor string. These events were not recorded by the lateral array, even though it was adjacent. The events registered by the lateral array are not recorded by the vertical array and vice versa.

The dimensions of the brine networks are not known, and neither is the separation between the thermistor and the brine network. However, it should be safe to assume that the thermistors are close to the network of connected brine pockets.

Figure 2.7 shows the event of March 5, 2003 (day 67) that was only registered by the Hydraprobe, and not by any of the separate thermistor arrays deployed that season. Despite an apparent large brine volume change (Backstrom and Eicken, 2006), neither the thermistor in the Hydraprobe nor the independent thermistor strings record any temperature change, even though the separation between the thermistor string operated by UAF and the Hydraprobe array was only about one meter. The apparent insensitivity of the Hydraprobe to register any significant temperature change is partly due to the fact that the Hydraprobe thermistor is located inside the body of the instrument. It should be noted here that while the thermistors measure the temperature of the ice that is in direct contact with the instrument, the thermistor in the Hydraprobe can, at best, be said to measure the average temperature of the ice surrounding the body of the instrument. Furthermore, the Hydraprobe does not measure the temperature of same the volume of ice as it measures the dielectric properties. It was seen above that a brine movement in one single network of connected brine pockets would not change the temperature of the surrounding ice other than in the immediate vicinity.

This leads to the conclusion that these events are brine movements in single networks of connected brine pockets, and as such, they are difficult to analyze since we do not know the dimensions, the distribution in the ice, nor the spatial relationship to the sensors of the networks of connected brine pockets.

A heat transport event observed on day 117 of 2003 (April 27) (Fig. 2.8) is of a

completely different magnitude, however. Not only is the event recorded by all three separate instrument arrays (Pringle et al., in press), the temperature records are longer and also more complex. This would indicate a series of concurrent events lagging each other in time and space.

The event recorded by the thermistor string differs from the event recorded by the Hydraprobe. The instruments are separated by about a meter, and they measure distinct processes within the ice: the thermistors measure only the temperature of the ice that is in direct contact with the instrument, while the Hydraprobe measures changes in the complex dielectric permittivity due to changes in the amount of brine over a volume of ~13cm^3.

By looking at the temperature record in Figure 2.8 it is possible to see that the temperature change starts in the ice interior. For this to be a gravity drainage event the ice needs to be porous. The bulk salinity data from the cores and the temperature data from the thermistor arrays were used to estimate the porosity of the ice. The cores give the salinity with a depth resolution of 0.1 meters at various discrete times during the experiment. A time-dependent salinity was derived from the cores, assuming a constant desalination rate. The temperatures recorded at 600 seconds and 0.1 meter intervals throughout the period are known. The two time series can be combined and the Cox and Weeks (1983) equation can be used to calculate the relative brine volumes in the ice throughout the period. The result is presented in Fig. 2.9.

It is apparent that the Hydraprobe has been enmeshed in porous (relative brine volume >50‰) ice the whole time, but at around April 27 the entire ice column above the Hydraprobe appears to pass the percolation threshold as proposed by Golden et al. (1998). This would create a hydrostatic head in the brine overlying the horizon in which temperatures are measured (Eide and Martin, 1975). At this point, brine pockets would be vertically and laterally interconnected over large scales (Cottier et al., 1999; Golden,

2001). Some brine networks reach only through part of the ice; others penetrate trough the entire thickness of the ice (Miner, 2007). The hydrostatic pressure at depth z in a brine network connected to the liquid ocean beneath the ice is described by the equation (Eide and Martin, 1975):

$$p_b(z) = g \int_z^{H_2(t)} \rho_b(T(z))dz \tag{2.1}$$

where:

$p_b(z)$ = the hydrostatic pressure

g = gravitational constant

$H_2(t)$ = height of the brine in the connective system, which can be higher than the thickness of the ice beneath the waterline

ρ_b = temperature dependent density of the brine calculated using Eqs. 2.2 and 2.3 (from Eicken, 2003)

$$\rho_b = 1 + 8 * 10^{-4} S_b \tag{2.2}$$

$$S_b = \left(1 - \frac{54.11}{T}\right)^{-1} \tag{2.3}$$

where:

S_b = the salinity of the brine in parts per thousand

T = temperature in °C

With a hydraulic head the entire brine network will drain downwards, letting cold, dense brine replace the warmer less dense brine below. For the brine to stay on the eutectic curve it must melt some of the surrounding ice (Eide and Martin, 1975; Niedrauer and Martin, 1979; Worster and Wettlaufer, 1997).

However, it should be noted here that the only actual measurement of change in porosity is the Hydraprobe measurement at 0.8 meters depth in the ice. Therefore, the exact porosity and brine movement in the ice above that level in not known. Even if it can be safely assumed that there is brine percolating at 0.8 meters depth and below, there is no clear indication of from where in the ice above the 0.8 meter level the percolating brine originates.

The thermistors do record a decrease in temperature, most pronounced at depths of 0.7 meters and below. Lower temperatures persist for about a day, followed by a similar abrupt increase in temperature. That would be commensurate with a downward movement of brine for as long as the hydraulic head persists. The cessation of the hydraulic head would leave the brine in the channels stagnant. If the networks of connected brine pockets are connected to the liquid ocean below the ice, there will still be a density gradient with cold saline brine overlaying the ocean. This is an unstable situation, therefore, a rapid oscillatory motion will commence, where the brine is gradually replaced by seawater, until the density gradient is removed (Martin, 1970). This will ensure a quick refreezing of the networks of connected brine pockets, resulting, as observed, in warming of the surrounding ice: both as a result of intrusion of warmer water from beneath the ice and as release of latent heat as it freezes.

The relation for calculating the relative brine volume and bulk salinity of the ice from the real part of the complex dielectric permittivity, derived in Backstrom and Eicken (2006) can now be used to calculate the initial change in relative brine volume.

$$\frac{V_b}{V} = -0.0582 + 0.0113 * \varepsilon' \qquad (2.4)$$

where:

V_b/V = the relative brine volume

ε' = the real part of the complex dielectric permittivity

The change in relative brine volume is 10 ‰ (Fig. 2.8). That would translate into an actual change of 0.13 cm^3 inside the measurement volume of the Hydraprobe.

As the brine percolates downwards through the ice and is no longer in equilibrium with the surrounding ice a heat transfer with two components will develop: one part consists of heat from the surrounding ice flowing to the brine to heat it (thereby cooling the ice), and the other part is due to melting of the ice surrounding the network of connected brine pockets (Eide and Martin, 1975). The relation developed by Eide and Martin (1975) is:

$$\frac{Q_s}{Q_t} = \alpha = \frac{L\rho_i m_1}{\rho c s_o} \tag{2.5}$$

where:

L = the latent heat of the ice

ρ_i = the density of the ice (= 0.92 gcm^{-3})

m_1 = the change in salinity of the brine per degree centigrade along the eutectic curve (10 $‰T^{-1}$)

s_o = the original salinity of the brine in ‰, when it was at eutectic equilibrium

Q_s = Latent heat due melting or freezing

Q_t = Sensible heat due to temperature difference between brine and surrounding ice

c = specific heat capacity of the brine (= 3.8 Jg^{-1})

The equation for the release/absorption of latent heat is:

$$Q_{Latent} = \rho_i LV \tag{2.6}$$

where:

V = change in volume in cm^{-3} from freezing of brine or melting of ice

ρ_i = the density of the ice (= 0.92 gcm^{-3})

L = the latent heat of sea ice in $Jg^{-1}K^{-1}$ (Yen et al., 1991):

$$L = 4.187 * \left(79.68 - 0.505T - 0.0273S_i + 4.3115\frac{S_i}{T} + 0.0008S_iT - 0.009T^2 \right) \quad (2.7)$$

where:

T = the temperature in °C

S_i = the bulk salinity of the ice in parts per thousand (‰)

Using an ice temperature of -3°C, and an ice salinity of 5 ‰ will give a latent heat of 318 Jg^{-1}. If it is assumed that the brine comes from directly above the Hydrapobe it will have a salinity of 70 ‰. Then, using Eq. 2.5 gives $\alpha = 10$. Therefore the sensible cooling and warming of the ice can be ignored for the purpose of this study.

Insertion in Eq. 2.6 gives Q_{latent} a value of 38 J. The equation for the sensible heating/cooling of the surrounding ice is:

$$Q_{Sensible} = \rho_i c_i \Delta T V \quad (2.8)$$

where:

T = change in ice temperature in °C

V = volume of affected ice in gcm^{-3}

With Untersteiner's parameterization of the specific heat capacity of sea ice (Maykut, 1986):

$$c_i = 2.113 + 17.2\frac{S_i}{T^2} \tag{2.9}$$

where:

T = change in ice temperature in °C

S_i = the bulk salinity of the ice in parts per thousand (‰)

c_i = the temperature dependents heat capacity of sea ice

Insertion gives an estimated change in temperature due to the brine melting the surrounding ice to stay on the eutectic curve of –0.4 K. The thermistor strings record temperature changes of up to –0.6 K and, again, the thermistor in the Hydraprobe hardly records any temperature change at all. It should be noted here that the thermistor in the Hydraprobe is located in the body of the instrument. Therefore, the Hydraprobe measure the temperature and dielectric permittivity of two different, but adjacent, volumes of the ice. This would indicate that the networks of connected brine channels are discrete heat sources/sinks within the ice matrix, and that the heating/cooling is not even throughout the ice sheet. At this point, the actual distribution of brine networks in the interior of the ice is not known, for further details see Miner et al (2007).

2.4.2. Analysis of heat flow

The second step of the analysis is to investigate the effect these events of brine percolation have on the energy budget of the ice. For a full overview of the energy budget of sea ice, see Wadhams (2000).

It is possible to use the temperature data from the thermistors, and the ice thickness

measurements, as obtained from the thermistor data and compared with data from nearby cores. This information makes it possible to use Fourier's law of thermal conductivity in one dimension:

$$F_c = -\lambda \frac{\Delta T}{\Delta z} \tag{2.10}$$

where:

F_c = heat flow through the ice sheet in $Jm^{-2}S^{-1}$

λ = thermal conductivity in $Wm^{-1}K^{-1}$

Since the salinity and temperature were measured or derived at intervals of 0.1 meters and 600 seconds, it was possible to use the Untersteiner parameterization (Maykut, 1986) to estimate the conductivity of the ice at 0.1 meter depth intervals:

$$\lambda_{si} = \lambda_i + 0.13 \frac{S_i}{T} \tag{2.11}$$

where:

S_i = bulk salinity of the ice in parts per thousand (‰)

T = temperature of the ice in °C

λ_{si} = thermal conductivity of sea ice in $Wm^{-1}K^{-1}$

λ_i = thermal conductivity of pure ice in $Wm^{-1}K^{-1}$

$$\lambda_b = 1.16 * (1.91 - 8.66 * 10^{-3} T + 2.97 * 10^{-5} T^2) \quad (2.12)$$

where:

T = temperature of the ice in °C

The expression in Eq. 2.12 for the conductivity of pure ice is from Yen et al. (1991). Using salinity data from cores and Eqs. 2.11 and 2.12 an average thermal conductivity, $\lambda = 2.0$ $Wm^{-1}K^{-1}$ for the ice was established.

To remove the effect of radiative heating of the surface the heat flow was measured between the bottom of the ice, considered to be at constant temperature of –1.86°C, and every 0.1 meters up to the depth level of 0.5 meters below the upper surface. This was only possible to do for season 2002/2003 since the actual thickness of the ice during the 1999/2000 season could not be determinated, possibly due to malfunctioning thermistors in the lower layers of the ice preventing identification of the ice-water interface.

Niedrauer and Martin (1979) and Worster and Wettlaufer (1997) showed that there is a constant convection in the skeletal layer in the ice at the boundary to the ocean below. The effect on the heat flow of the ice from this boundary-layer convection cannot be isolated from the conductive heat flow. However, the contribution is not considered to be significant (Niedrauer and Martin, 1979; Pringle et al., in press).

Only the event of April 27 2003 was analyzed, see Fig. 2.10. It is apparent that the heat flow increases, at depths of 0.8 meters in the ice and below. Above 0.8 meters depth, the effect is gradually damped, until at 0.5 meters depth in the ice it is not noticeable. That could indicate that whatever happens during the brine percolation event, it happens at and below the 0.8 meter depth in the ice. This finding could be explained such that there is no brine percolation in the upper reaches of the ice, or there is, but it is not being

captured by the instruments. At present, neither the size nor the distribution of the interconnected brine channel networks have been recorded to the extent that it would allow firm conclusions about the potential for drainage of brine from the upper surface down into the ice. This is partly due to the fact that with only one Hydraprobe deployed, little is known about brine drainage in the upper levels of the ice.

2.5 Discussion and conclusion

Brine percolation and drainage events during the ice growth season appear to be rare, and only affect the immediate vicinity of the discrete network of connected brine pockets. The one event that was registered by more than one instrument (on April 27, 2003 (day 117)) does not appear to have any significant effect on the total heat flow. Due to the scarcity of recorded events, it was not possible to establish a statistical correlation between the brine drainage events and changes in temperaure in the ice.

Measurements with several instrument strings deployed in parallel indicate that the distribution of drainage events is not homogenous. The effect of the majority of the observed events is localized and of short duration. The present lack of understanding of the dimensions and distribution of the networks of connected brine channels makes it difficult to analyze events registered by thermistors only, since the spatial relationship between the thermistor and the network of connected brine channels is not known.

We see that the apparent cause of the event of April 27, 2003 (day 117) was a sudden transition of the ice freeboard layer from a state of low to high permeability, allowing brine to drain. However, even though a similar transition appears in the record for the 2001/2002 season, no brine movement was apparent from the temperature record. This should indicate that not all mechanisms for brine movement in first year sea ice are

known. A better understanding of the brine movement mechanisms can be obtained by using vertical arrays of Hydraprobes, which can detect changes in the composition and microstructure of the ice.

Examining the heat flow during the event of April 27 2003 it can be seen that the heat flow increase is confined to depths of 0.8 meters and below in the ice. The effect decreases rapidly above 0.8 meters depth, and appears absent at 0.5 meters depth. Neither does the event appear to have any effect on the overall trend in the bulk heat flow. Without detailed knowledge of the percolation of brine in the ice, or the distribution and dimensions of the networks of connected brine pockets, it is not possible to provide a full explanation of this observation. However, it appears that the brine movement is confined to the region around and below 0.8 meters depth. There the latent heat absorbed, and later released, is not sufficient for a substantial change in temperature of the ice - possibly due to low volume density of networks of connected brine channels.

2.6 Figures

A

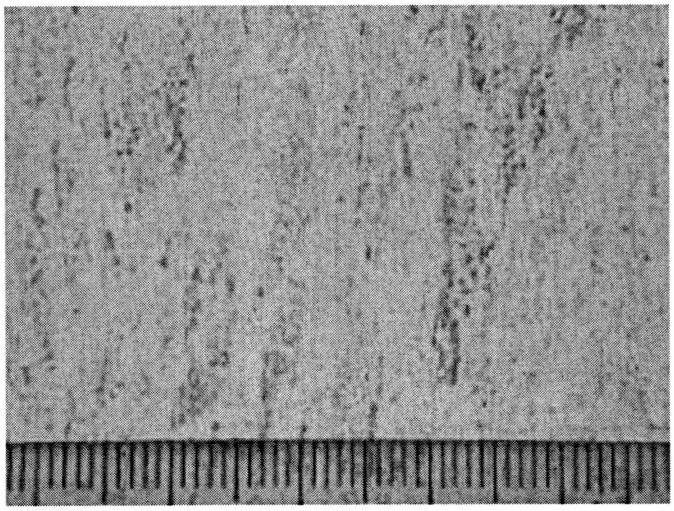

B

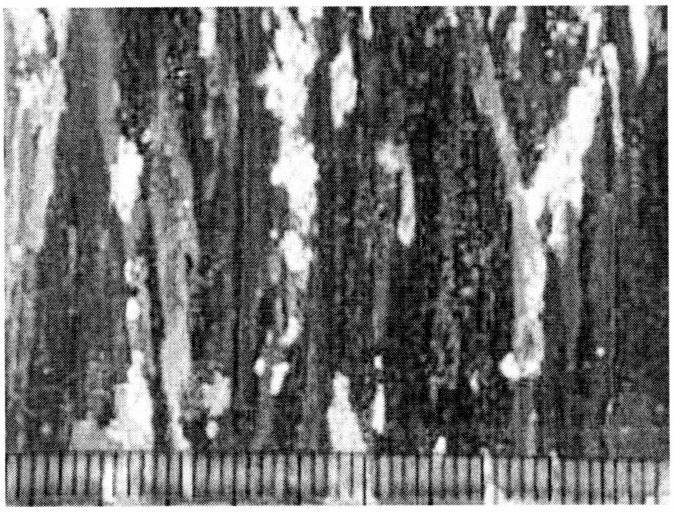

A

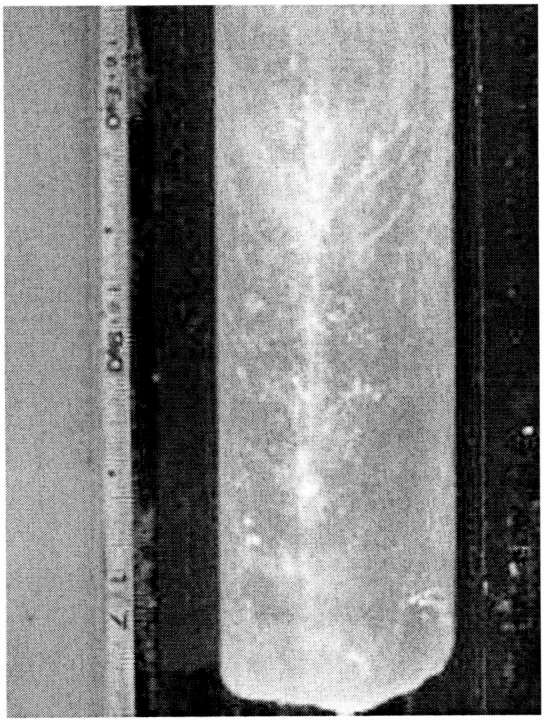

B

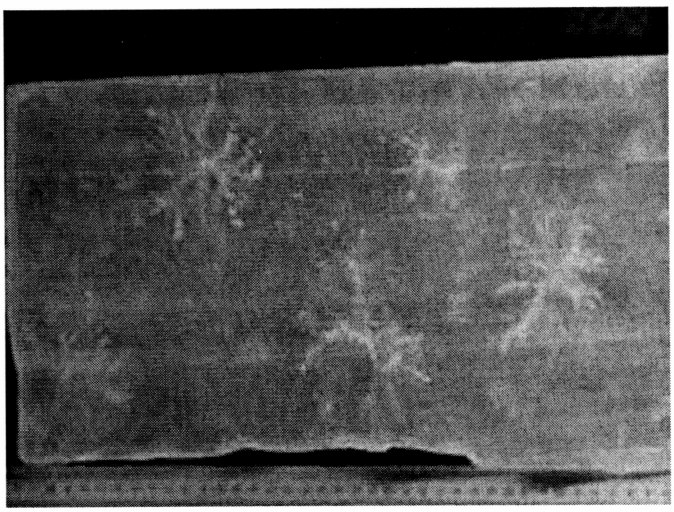

Fig. 2.3. The mass balance site in the Chukchi Sea. Barrow, February 3, 2003 (Photo A. Mahoney).

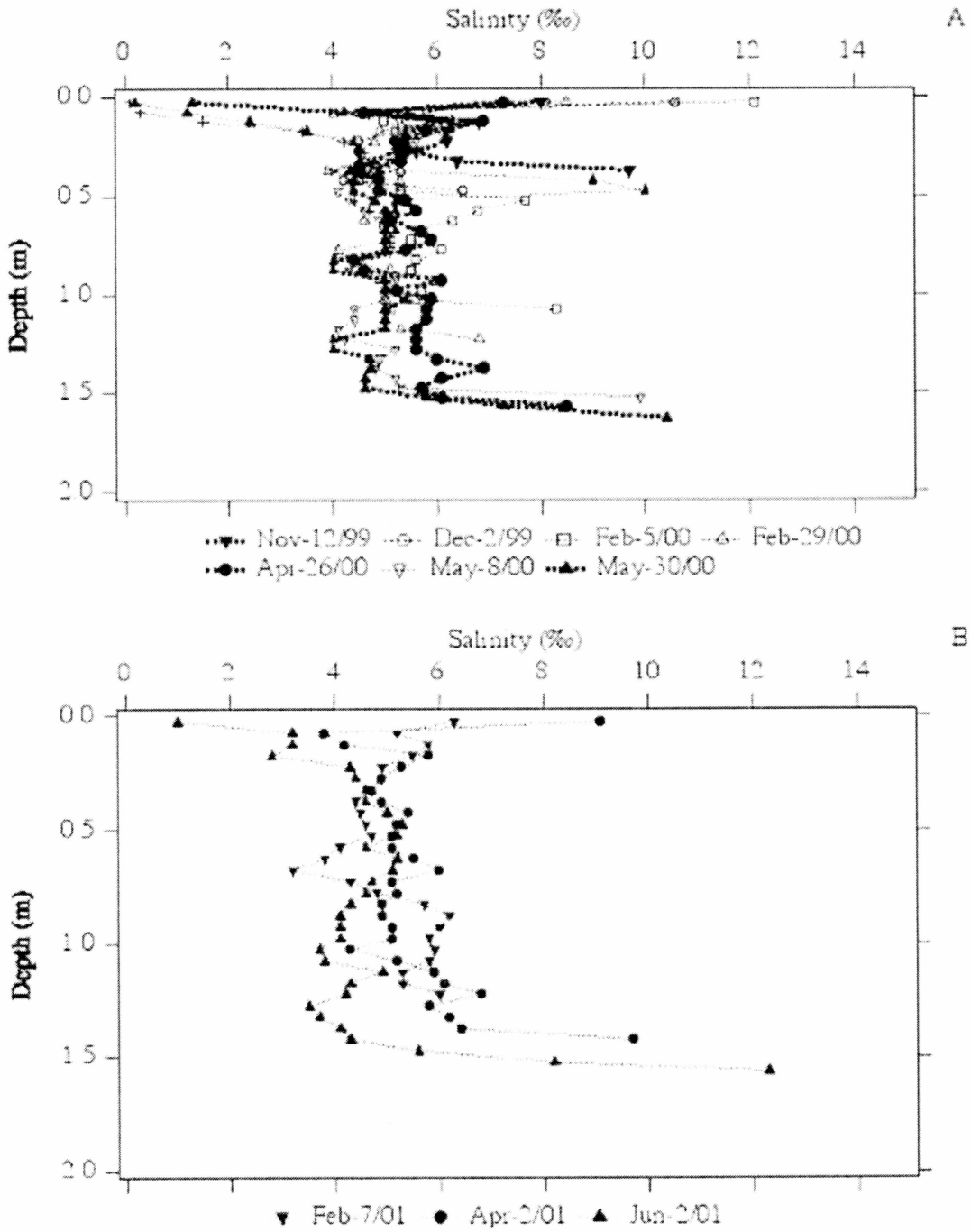
A
Salinity (‰)
0
2
4
6
8
10
12
14
0.0
0.5
1.0
1.5
2.0
Depth (m)
Nov-12/99
Dec-2/99
Feb-5/00
Feb-29/00
Apr-26/00
May-8/00
May-30/00
B
Salinity (‰)
Depth (m)
Feb-7/01
Apr-2/01
Jun-2/01

C

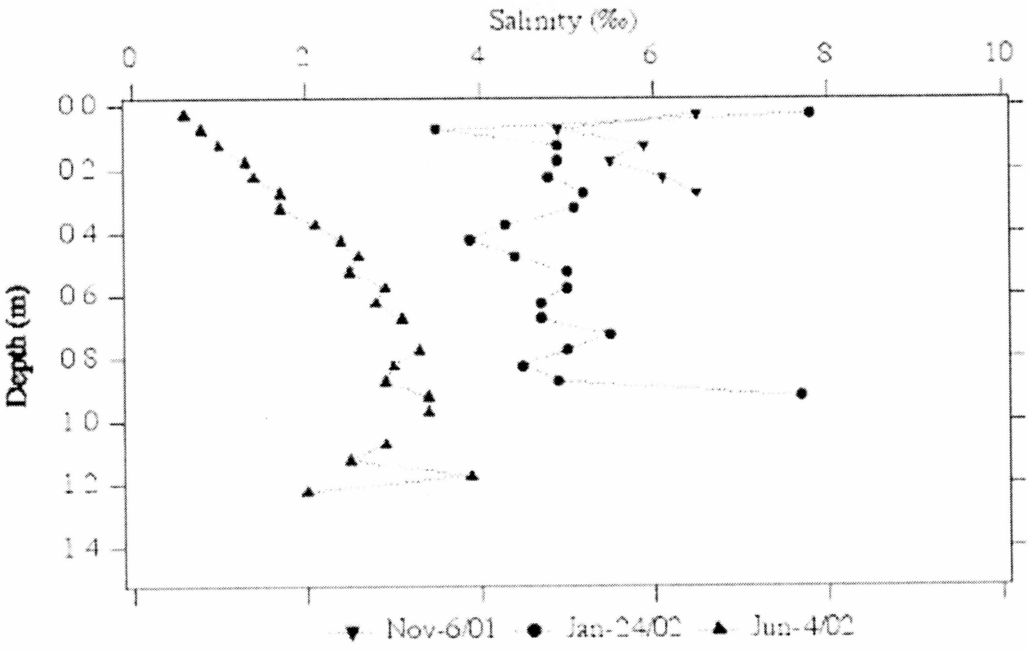
Salinity (‰)
0
2
4
6
8
10
0.0
0.2
0.4
0.6
0.8
1.0
1.2
1.4
Depth (m)
Nov-6/01
Jan-24/02
Jun-4/02

D

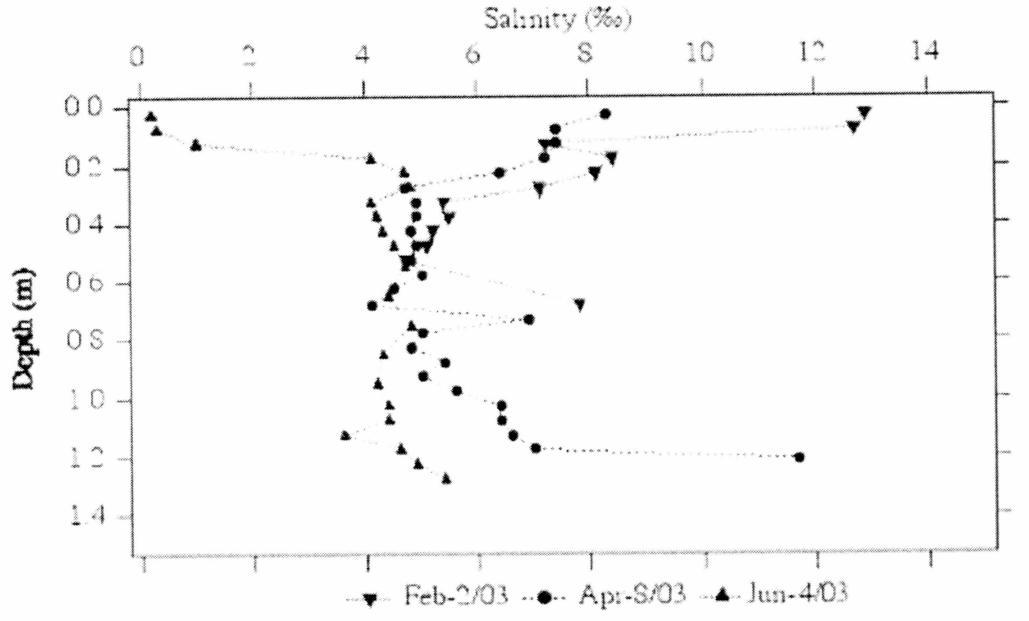
Salinity (‰)
0
2
4
6
8
10
12
14
0.0
0.2
0.4
0.6
0.8
1.0
1.2
1.4
Depth (m)
Feb-2/03
Apr-8/03
Jun-4/03

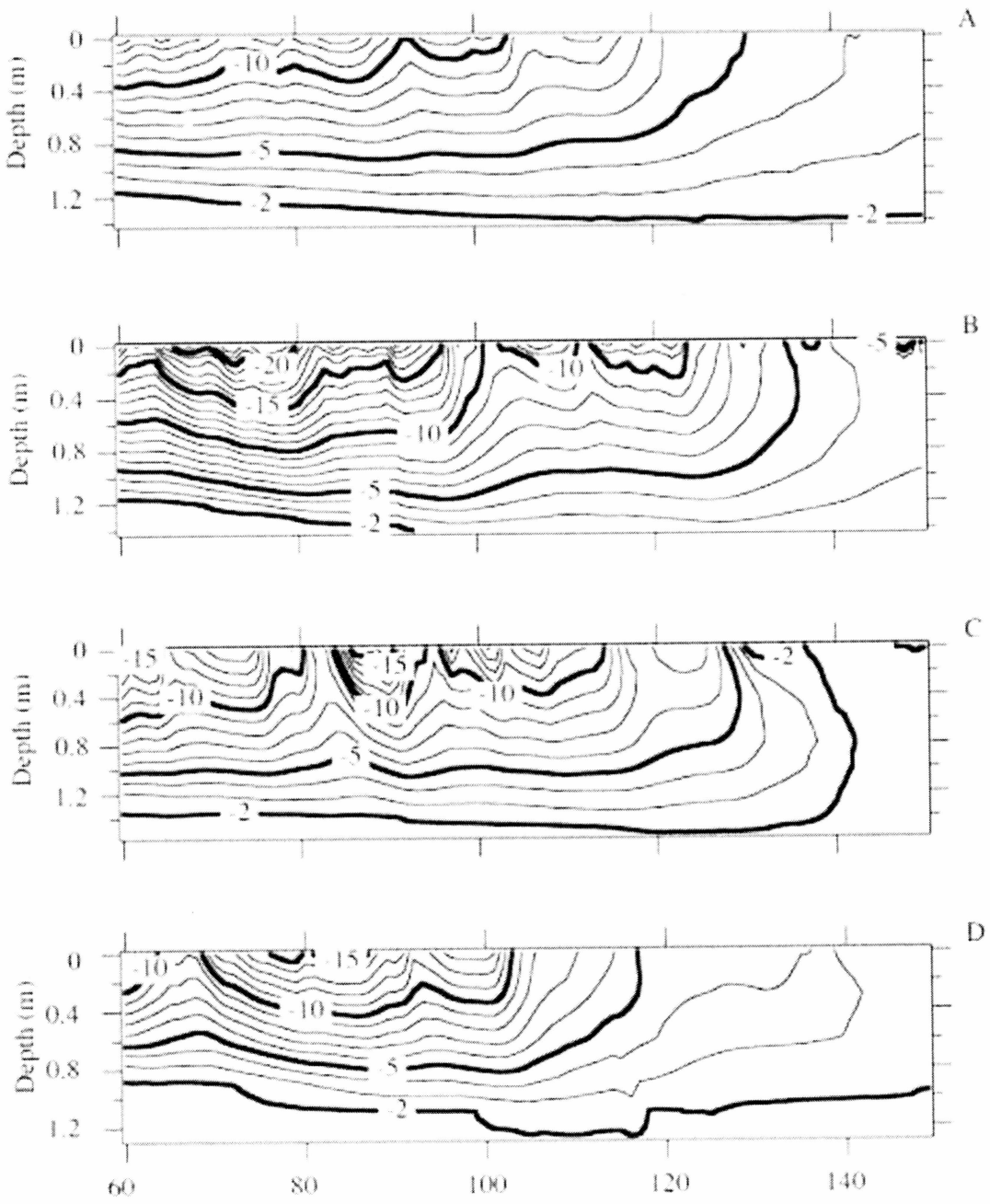
A
B
C
D
Depth (m)
0
0.4
0.8
1.2
-20
-15
-10
-5
-2
60
80
100
120
140

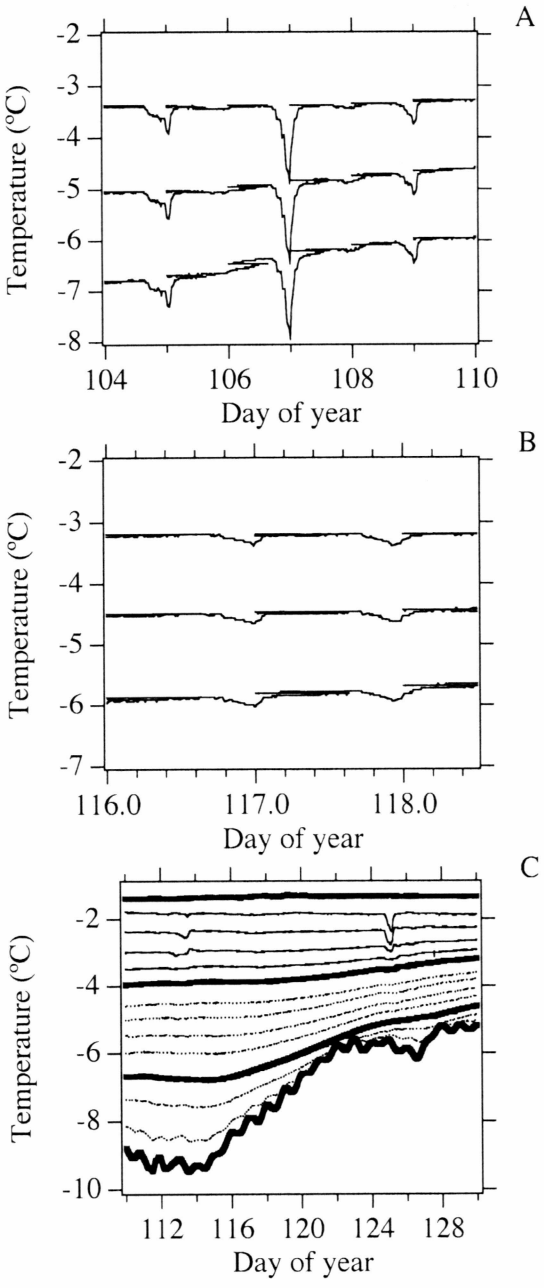
A
-2
-3
-4
-5
-6
-7
-8
Temperature (°C)
104
106
108
110
Day of year
B
-2
-3
-4
-5
-6
-7
Temperature (°C)
116.0
117.0
118.0
Day of year
C
-2
-4
-6
-8
-10
Temperature (°C)
112
116
120
124
128
Day of year

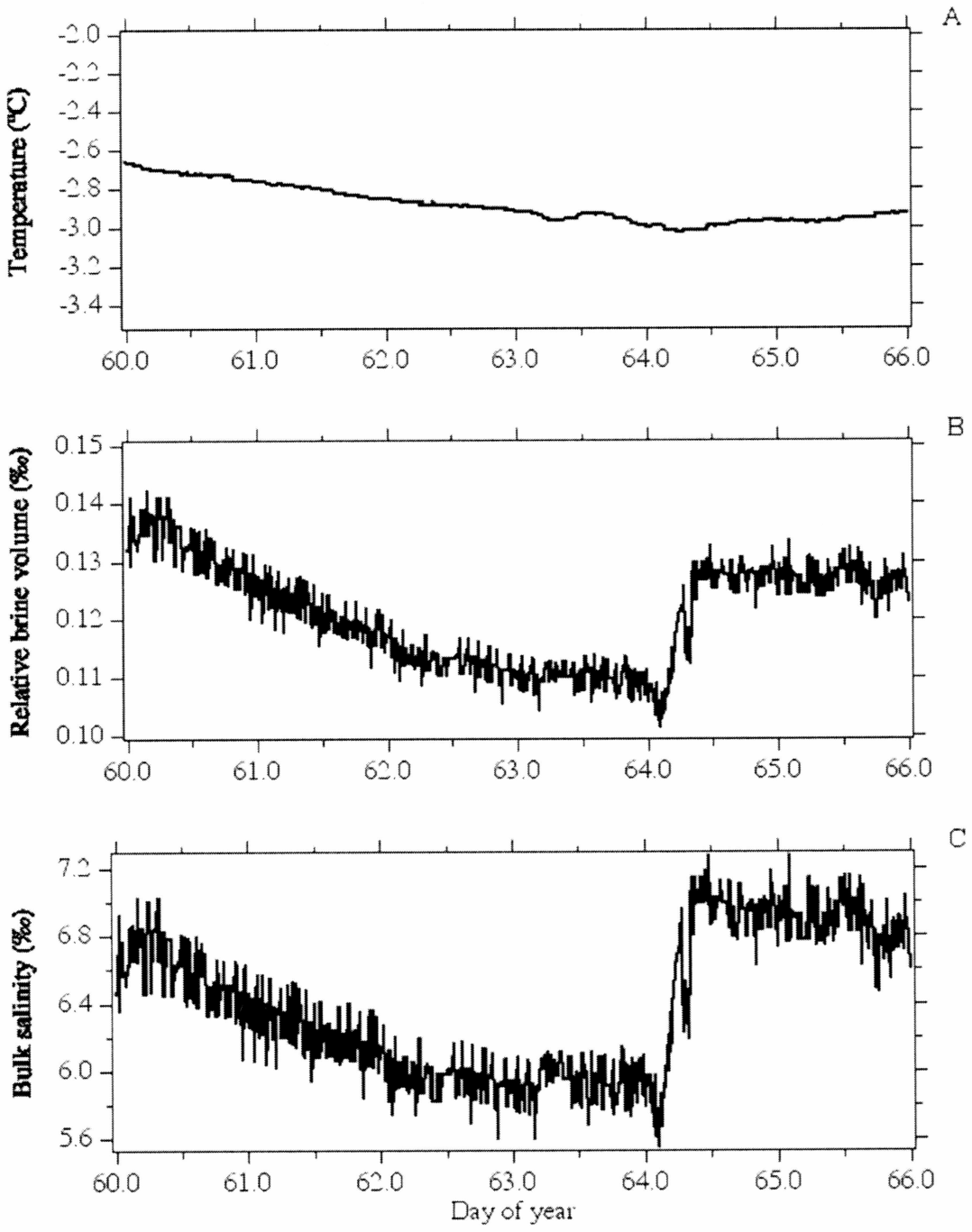
A
Temperature (°C)
-2.0
-2.2
-2.4
-2.6
-2.8
-3.0
-3.2
-3.4
60.0
61.0
62.0
63.0
64.0
65.0
66.0
B
Relative brine volume (‰)
0.15
0.14
0.13
0.12
0.11
0.10
C
Bulk salinity (‰)
7.2
6.8
6.4
6.0
5.6
Day of year

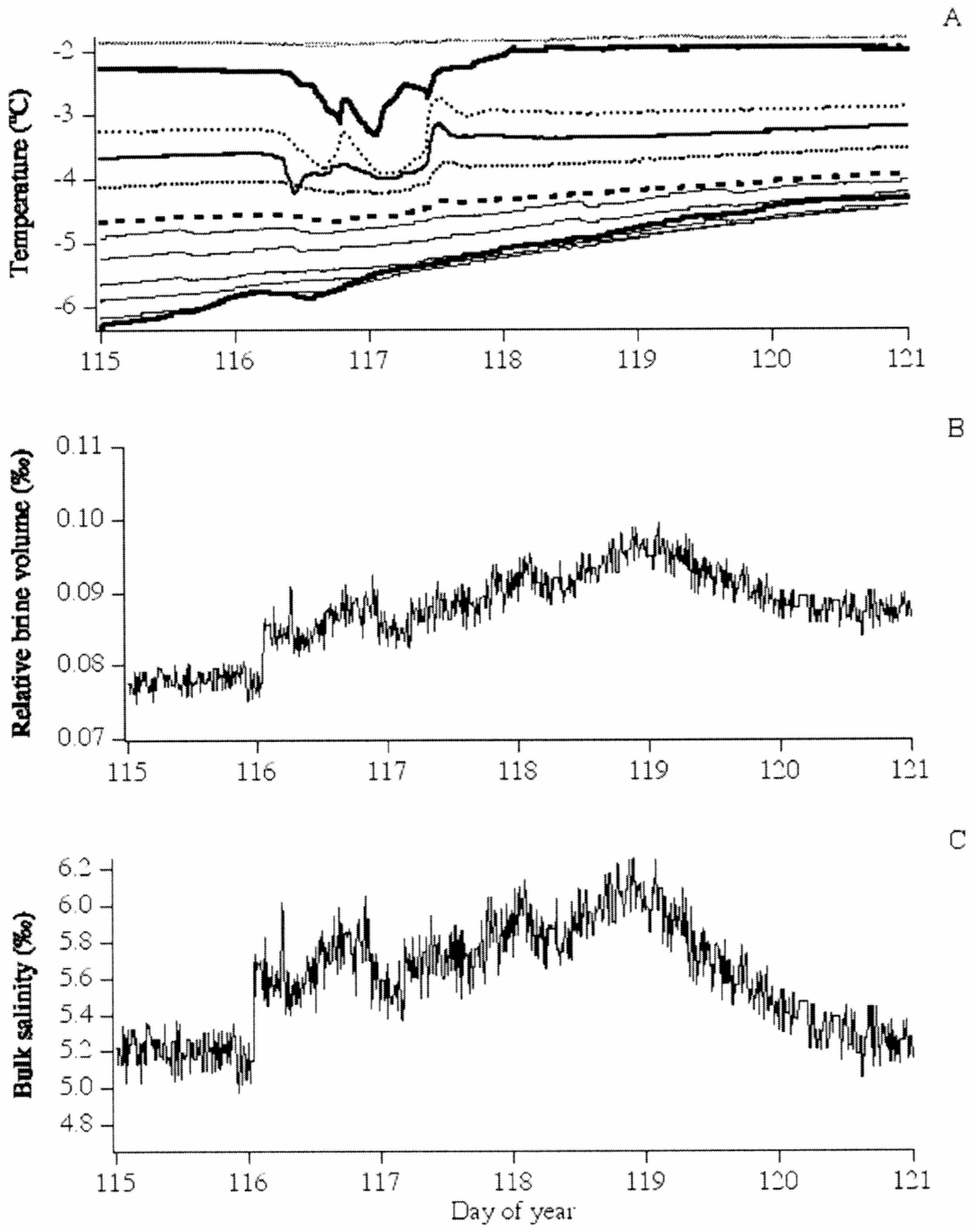
A
Temperature (°C)
-2
-3
-4
-5
-6
115
116
117
118
119
120
121
B
Relative brine volume (‰)
0.11
0.10
0.09
0.08
0.07
115
116
117
118
119
120
121
C
Bulk salinity (‰)
6.2
6.0
5.8
5.6
5.4
5.2
5.0
4.8
115
116
117
118
119
120
121
Day of year

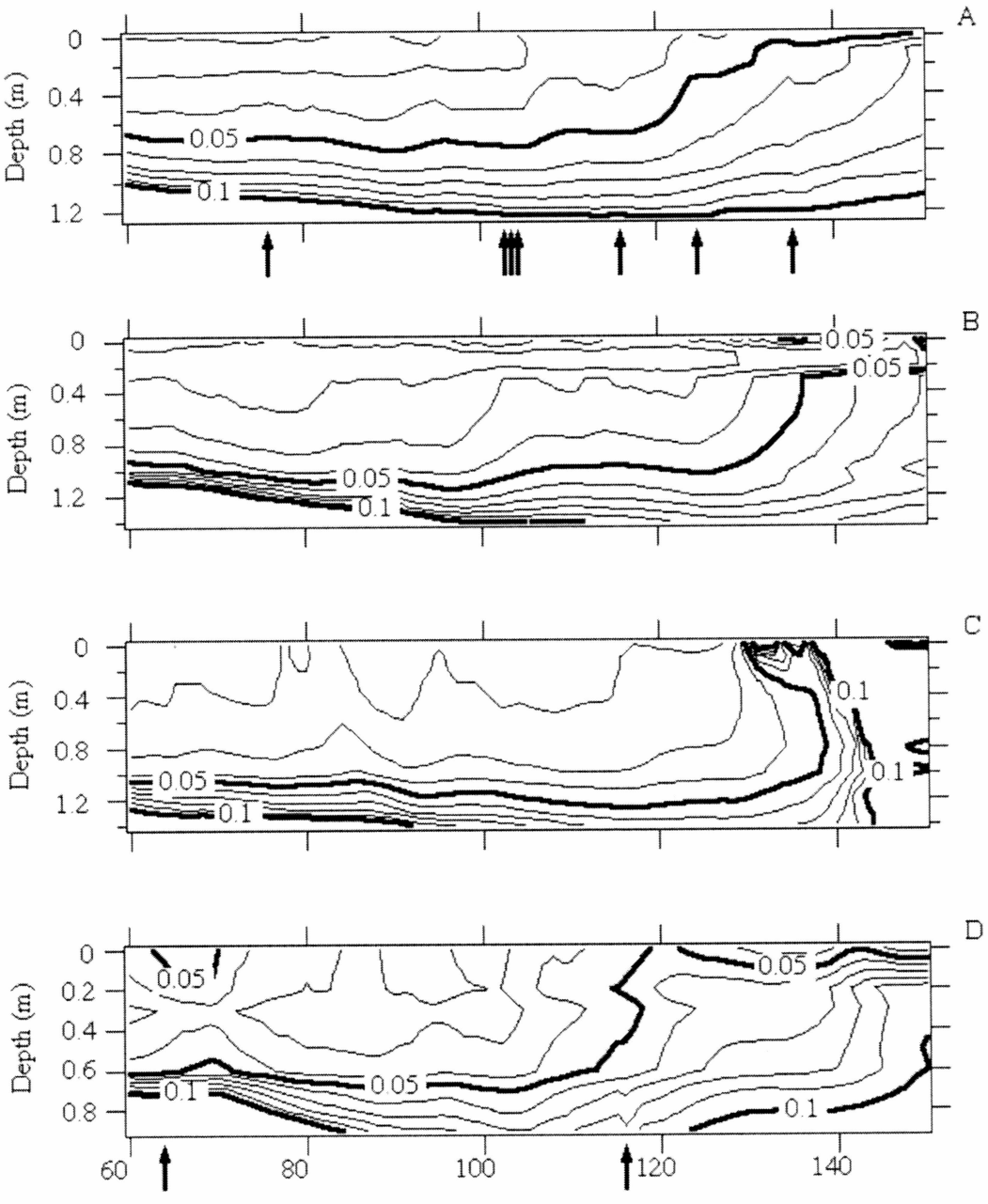
A
B
C
D
Depth (m)
0
0.4
0.8
1.2
0.2
0.6
0.05
0.1
60
80
100
120
140
Day of year

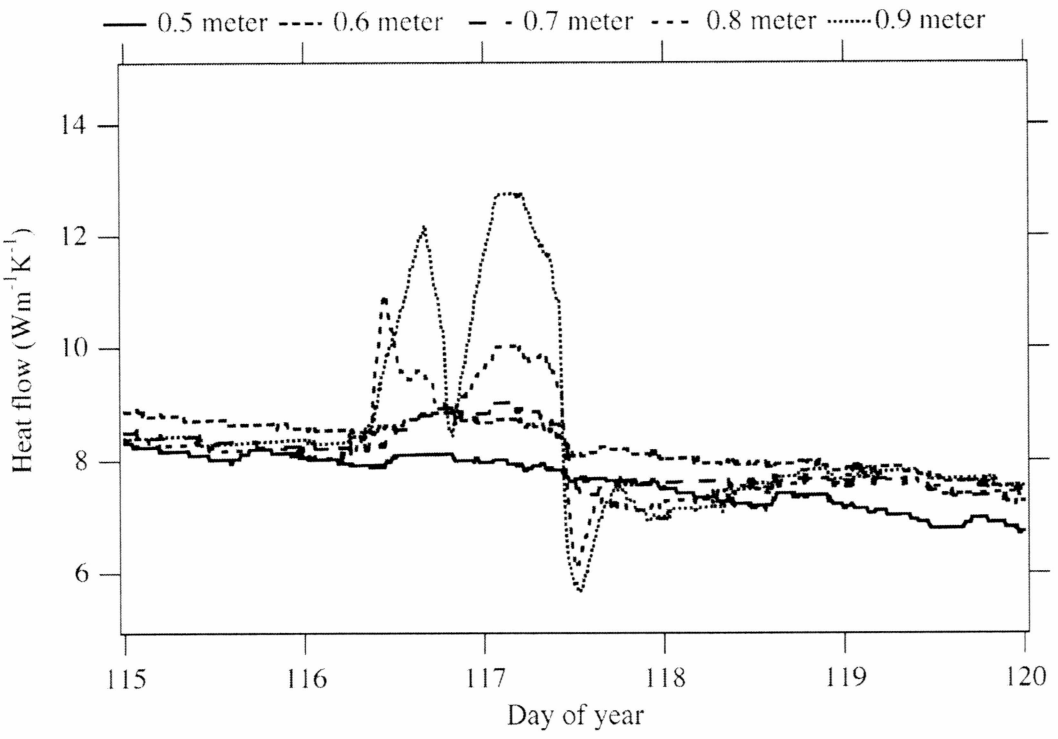

Fig. 2.10. Graph showing the calculated heat flow in the ice during and around the time of the brine drainage event of April 27 2003. Before and after the event the heat flow is constant throughout the thickness of the ice. During the event the flow increases dramatically at depths of 0.8 meter and below. However, at around 0.5 meters depth in the ice, the event is barely perceivable in the graph.

2.7 Tables

Table 2.1. Mass balance and instrument array sites in the landfast undeformed first-year sea ice in the Chukchi Sea outside Barrow.

Season	Location		Notes
1999/2000	71°19.64'N	156°42.13'W	Vertical and lateral thermistor arrays
2000/2001	71°19.62'N	156°41.40'W	
2001/2002	71°21.26'N	156°31.42'W	Four vertical thermistor arrays in three
	71°19.64'N*	156°42.13'W*	locations, two of them at*
	71°19.62'N	156°41.40'W	
2002/2003	71°20.24'N	156°40.12'W	One vertical thermistor array and one Hydraprobe array operated by UAF and a vertical thermistor array operated by VUW

Table 2.2. Mass balance data from cores. Note that the cores from the 2000/2001 season were not obtained from the actual mass balance site, but from a point just off the beach outside UIC-NARL.

Date	11/12/99	2/5/00	2/29/00	4/26/00	5/8/00	5/30/00
Snow depth (m)	0.025	0.19	0.05	0.05	0.15	0.15
Freeboard (m)	0.04	0.04	0.095	0.095	0.12	0.09

Date	4/2/01	6/2/01
Snow depth (m)	0.035	0
Freeboard (m)	0.12	0.14

Date	11/6/01	1/24/02	6/4/02
Snow depth (m)	0.04	0.04	0.02
Freeboard (m)	N/A	0.05	0.1

Date	2/2/03	4/8/03	6/5/03
Snow depth (m)	0.03	0.02	0
Freeboard (m)	0.09	0.09	0.12

2.8 References

Backsrom, L. G. E. and Eicken, H., 2006. Capacitance probe measurements of brine volume and bulk salinity in first-year sea ice, Cold Regions Science and Technology, doi:10.1016/j.coldregions.2006.08.018.

Bennington, F., 1967. Desalination features in natural sea ice. Journal of Glaciology, 6(48): 845-857

Cole, D. M. and Shapiro, L. H., 1998. Observations of brine drainage networks and microstructure of first-year sea ice. Journal of Geophysical Research, 103(C10): 21739-21750

Cottier, F., Eicken, H. and Wadhams, P., 1999. Linkages between salinity and brine channel distribution in young sea ice. Journal of Geophysical Research, 104(C7): 15859-15871

Cox, G. F. N. and Weeks, W. F., 1983. Equations for determining the gas and brine volumes in sea-ice samples. Journal of Glaciology, 29(102): 306-316

Eicken, H., Cole, D. M., Backstrom, L. G. E., Pringle, D., Shapiro, L. H., and Trodahl, J., in preparation. Permeability-porosity relationships and convective heat transfer in first-year Arctic sea ice. Journal of Geophysical Research

Eide, L. I. and Martin, S., 1975. The formation of brine drainage features in young sea ice. Journal of Glaciology, 14(70): 137-154

Golden, K. M., 2001. Brine percolation and the transport properties of sea ice. Annals of Glaciology, 33: 28-35

Golden, K. M., Ackley, S. F. and Lytle, V. I., 1998. The percolation phase transition in sea ice. Science, 282: 2238-2241

Lake, R. A. and Lewis, E. L., 1970. Salt rejection by sea ice during growth. Journal of Geophysical Research, 75(3), 583-597

Malmgren, F., 1927. On the properties of sea ice. The Norwegian North Pole Expedition with the "Maud" 1918-1925. Scientific Results, Vol. 1, No. 5

Martin, S., 1970. A hydrodynamic curiosity; the salt oscillator. Geophysical Fluid Dynamics, 1: 143-160

Maykut, G. A., 1986. The surface and mass balance. In: Untersteiner (Ed.), The geophysics of sea ice. Plenum press, NY. pp. 395-463

Miner, J., 2007. Connectivity and morphology of brine inclusions in first year sea ice. Unpublished MS thesis, University of Alaska Fairbanks, USA

Niedrauer, T. M., and Martin, S., 1979. An experimental study of brine drainage and convection in young sea ice. Journal of Geophysical Research, 84(C3): 1176-1186

Pringle, D. J., Eicken, H., Trodahl, H.J. and Backstrom, L., in press. Thermal conductivity of land-fast Antarctic and Arctic sea ice. Journal of Geophysical Research

Tucker, W. B., Gow, A. J. and Richter, J. A., 1984. On small-scale horizontal variations of salinity in first-year sea ice. Journal of Geophyiscal Research, 89(C4): 6505-6514

Wadhams, P., 2000. Ice in the ocean. Gordon and Breach Science Publishers, London, UK. Pp.81-109

Wakatsuchi, M. and Kawamura, T., 1987. Formation processes of brine drainage channels in sea ice. Journal of Geophysical Research, 92(C7): 7195-7197

Wakatsuchi, M. and Saito, T., 1985. On brine drainage channels of young sea ice. Annals of Glaciology, 6: 200-202

Weeks, W. F. and Ackley, S. F, 1986. The growth, structure and properties of sea ice. In: Untersteiner, N. (Ed.), The geophysics of sea ice. Plenum press, NY. pp. 9-164

Worster, M. G. and Wettlaufer, J.S., 1997. Natural convection, solute trapping, and channel formation during solidification of saltwater. Journal of Physical Chemistry B, 101(32): 6132-6136

Yen, Y. C., Cheng, K. C., and Fukusako, S., 1991. Review of intrinsic thermophysical properties of snow, ice, sea ice, and frost. In: Proceedings 3rd international symposium on cold regions heat transfer, Fairbanks, AK, June 11-14, 1991. Zarling, J. P. and Faussett, S. L., (Eds.). University of Alaska Fairbanks, AK. pp. 187-218

General Conclusions

The first chapter of this thesis describes a non-destructive method to measure the in situ bulk salinity and brine volume fraction of sea ice. This approach relies on commercially available capacitance probes (Stevens Water Systems Hydraprobes) that are frozen into the ice to determine the complex dielectric permittivity measurements at 50 MHz.

By retrieving cores, from which bulk salinity was obtained throughout the experiments, it was possible to develop a correlation between relative brine volume, bulk salinity, temperature and the real part of the complex dielectric permittivity of the ice.

The relation that was developed is valid for columnar bubble free ice that has not experienced flushing yet, and where the brine inclusions can be modeled as discrete ellipsoids. These conditions correspond well to the interior of first-year, undeformed sea ice below the percolation threshold.

At present, the relation gives the bulk salinity of the ice as a function of temperature and the real part of the complex dielectric permittivity, with an error limit of 15 % below the percolation threshold, and 25 % above the percolation threshold, but below relative brine volumes of 100 ‰. These error limits can be improved upon in conjunction with future experiments, especially by more detailed measurements of bulk salinity from ice cores.

In the approach to derive the relative brine volume and bulk salinity developed here, only the real part of the complex dielectric permittivity was relied upon, with the morphology of brine inclusions estimated as a function of ice type and temperature based

on previous work. By also incorporating the imaginary part of the complex dielectric permittivity into the analysis, the method described in this thesis can be employed to determine the morphology of the brine inclusions. Further experiments that include ice microstructural characterization from thin sections and non-destructive techniques as well as improved dielectric mixture models (Gully et al., in press) would allow for an extension of the present approach to estimate bulk salinity and relative brine volume of other types of ice, e.g. frazil, platelet, and multi-year ice. These types of ice have more complex crystal and brine inclusion morphology. Air bubbles might also be present.

In the first chapter of the thesis it was observed that gravity drainage of brine occurred during a period when radiative heating in early spring warmed the upper surface of the ice, and possibly, causing the entire ice thickness to become permeable to brine. As far as it can be ascertained from literature, this phenomenom not been previously observed. Cox and Weeks (1975) showed that the main mechanism for desalination in first-year sea ice is gravity drainage. However, in their experiment the ice was cooled from above, and radiative heating was not simulated.

The second chapter of this thesis, therefore, examines the mechanism for gravity drainage and the effect it has on the surface energy budget of the ice. Data from several seasons of ice temperature measurements made at mass-balance sites in the landfast ice outside of Barrow, Alaska are used.

During four years of experiments, only one gravity-drainage event that was recorded by more than one array was observed (April 27TH 2003). Further investigations of the

overall effect of gravity drainage events on temperature showed that not even this single large event had any noticeable effect on the energy budget of the ice.

To be able to properly observe the distribution of brine in the ice and associated gravity drainage processes, it is necessary to have both vertical and horizontal arrays of instruments in place that measure the temperature and complex dielectric permittivity of the ice. Comparisons with studies by Miner (2007) will also help with determining the dimensions and number density of these interconnected networks of brine inclusions.

Even though it appears that it is a necessary condition for the entire ice thickness to become permeable for deep-reaching gravity drainage events to occur, it does not seem to be a sufficient condition, since years without any such large-scale gravity drainage episodes are seen. Further studies are necessary to determine the exact conditions required for large-scale gravity drainage events to occur.

References

Aagard, K., Coachman, L.K. and Carmack, E. C., 1981. On the halocline of the Arctic Ocean. Deep Sea Res., 28A(6), 529-545

Bennington, F., 1967. Desalination features in natural sea ice. Journal of Glaciology, 6(48): 845-857

Carmack, E. C., 2000. The Arctic Ocean's freshwater budget: sources, storage and export. In: Eds. L. Lewis, E. P. Jones, P. Lemke, T. D. Prowse and P. Wadhams, The Freshwater Budget of the Arctic Ocean. Kluwer, the Netherlands, pp. 91-126

Comiso, J. C., 2003. Large-scale characterisics and variability of the global sea ice cover. In: Eds. D. N Thomas and G. S. Dieckmann, Sea ice - an introduction to its physics, chemistry, biology and geology. Blackwell, Oxford, UK, pp. 112-143

Cox, G. F. N. and Weeks, W. F., 1975. Brine drainage and initial salt entrapment in sodium chloride ice. CRREL Report, 354. U. S. Army Cold Regions Research and Engineering Laboratory, Hanover, NH

Cox, G. F. N. and Weeks, W. F., 1988. Numerical simulations of the profile properties of undeformed first-year sea ice during the growth season. Journal of Geophyiscal Research, 93(C10): 12449-12460

Dieckmann, G. S. and Hellmer H. H., 2003. The importance of sea ice: an overview. In: Eds. D. N Thomas and G. S. Dieckmann, Sea ice - an introduction to its physics, chemistry, biology and geology. Blackwell, Oxford, UK, pp. 1-22

Ebert, E. E. and Curry, J. A., 1993. An intermediate one-dimensional thermodynamic sea ice model for investigating ice atmosphere interactions. Journal of Geophysical Research, 98(6): 10085-10109

Eicken, H., 2003. From the microscopic to the macroscopic, to the regional scale: growth, microstructure and properties of sea ice. In: Eds. D. N Thomas and G. S. Dieckmann, Sea ice - an introduction to its physics, chemistry, biology and geology. Blackwell, Oxford, UK, pp. 22-82

Eide, L. I. and Martin, S., 1975. The formation of brine drainage features in young sea ice. Journal of Glaciology, 14(70): 137-154

Eppler, D.T., Farmer, L.D., Lohanick, A.W., Anderson, M.A., Cavalieri, D., Comiso, J., Gloersen, P., Garrity, C., Grenfell, T.C., Hallikainen, M., Maslanik, J.A., Mätzler, C., Melloh, R.A., Rubinstein, I. and Swift. C.T., 1992. Passive microwave signatures of sea ice. In: Ed. F. Carsey. Microwave Remote Sensing of Sea Ice, Geophys. Monogr. Ser, (68). AGU, Washington, D.C., pp. 47-71

Fogg, G. E., 2003. Foreword. In: Eds. D. N Thomas and G. S. Dieckmann, Sea ice - an introduction to its physics, chemistry, biology and geology. Blackwell, Oxford, UK, pp. vii-xiii

Golden, K. M., Ackley, S. F. and Lytle, V. I., 1998. The percolation phase transition in sea ice. Science, 282: 2238-2241

Golden, K. M., 2001. Brine percolation and the transport properties of sea ice. Annals of Glaciology, 33: 28-35

Grenfell, T. C. and Maykut, G. A., 1977. The optical properties of ice and snow in the Arctic Basin. Journal of Glaciology 18(80): 445-463

Grenfell, T. C. and Perovich, D. K., 1984. Spectral albedos of sea ice and incident solar irradiance in the southern Beaufort Sea. Journal of Geophysical Research, 89(C3): 3573-3580

Grenfell, T. C., Cavalieri, D. J., Comiso, J. C., Drinkwater, M. R., Onstott, R. G., Rubenstein, I., Steffen, K. and Winebrenner, D. P., 1992. Considerations for microwave remote sensing of thin sea ice. In: Ed. F. Carsey. Microwave Remote Sensing of Sea Ice, Geophys. Monogr. Ser, (68). AGU, Washington, D.C., pp. 291-302

Gully, A., Backstrom, L. G. E., Eicken, H., and Golden, K., in press. Complex bounds and microstructural inversion for measurements of sea ice permittivity. Physica B

Hallikainen, M. and Winebrenner, D. P., 1992. The physical basis for sea ice remote sensing. In: Ed. F. Carsey. Microwave Remote Sensing of Sea Ice, Geophys. Monogr. Ser, (68). AGU, Washington, D.C., pp. 29-46

Kottmeier, C., and Sellmann, L., 1996. Atmospheric and Oceanic forcing of Weddell Sea ice motion. Journal of Geophysical Research, 101(C9). 20809-20824

Malmgren, F., 1927. On the properties of sea ice. The Norwegian North Pole Expedition with the "Maud" 1918-1925. Scientific Results, 1(5)

Maykut, G. A., 1982. Large-scale heat exchange and ice production in the central Arctic. Journal of Geophysical Research 87(C10): 7971-7984.

Miner, J., 2007. Connectivity and morphology of brine inclusions in first year sea ice. Unpublished M.S. thesis, University of Alaska Fairbanks, USA

Morey, R. M., Kovacs, A. and Cox, G. F. N., 1984. Electromagnetic properties of sea ice. CRREL Report, 80-20, U. S. Army Cold Regions Research and Engineering Laboratory, Hanover, NH

Niedrauer, T. M., and Martin, S., 1979. An experimental study of brine drainage and convection in young sea ice. Journal of Geophysical Research, 84(C3): 1176-1186

Ono, H., 1975. Thermal properties of sea ice IV. CRREL Draft Translation 467. CRREL, Hanover, N.H.

Onstott, R. G., 1992. SAR and scatterometer signatures of sea ice. In: Ed. F. Carsey. Microwave Remote Sensing of Sea Ice, Geophys. Monogr. Ser, (68). AGU, Washington, D.C., pp. 73-104

Perovich, D. K., 1990. The optical properties of sea ice. CRREL Monograph 96-1. CRREL, Hanover, N.H.

Perovich, D. K., 1994. Light reflecion from sea ice during the onset of melt. Journal of Geophysical Research, 99(C2): 3351-3359

Schwarzacher, W., 1959. Pack ice studies in the Arctic Ocean. Journal of Geophyiscal Research, 64(12): 2357-2367

Schwerdtfeger, P., 1963. The thermal properties of sea ice. Journal of Glaciology, 4(36): 789-807

Tucker, W. B., Gow, A. J. and Richter, J. A., 1984. On small-scale horizontal variations of salinity in first-year sea ice. Journal of Geophyiscal Research, 89(C4): 6505-6514

Untersteiner, N., 1968. Natural desalination and equilibrium salinity profile for perennial sea ice. Journal of Geophyiscal Research, 73(4): 1251-1257

Vant, M. R., 1976. A combined empirical and theoretical study of the dielectric properties of sea ice over the frequency range. Ph.D. Thesis, Carleton University, Ottawa, Canada

Weeks, W. F. and Ackley, S. F. 1986. The growth, structure and properties of sea ice. In: Ed. N. Untersteiner, The geophysics of sea ice. Plenum Press, New York, pp. 9-164

Weeks, W. F. and Assur, A., 1967. The mechanical properties of sea ice. Cold Regions Science and Engineering, part II, section C3. Hanover, N.H.

Worster, M. G. and Wettlaufer, J.S., 1997. Natural convection, solute trapping, and channel formation during solidification of saltwater. Journal of Physical Chemistry B, 101(32): 6132-6136